Hierarchical Language Model Design For Interpretable Graph Reasoning

Anonymous authors
Paper under double-blind review

Abstract

Large language models (LLMs) are being increasingly explored for graph tasks. Despite their remarkable success in text-based tasks, LLMs' capabilities in understanding explicit graph structures remain limited, particularly with large graphs. In this work, we introduce Hierarchical Language Model for Graph (HLM-G), which employs a two-block architecture to capture node-centric local information and interaction-centric global structure, effectively enhancing graph structure understanding abilities. The proposed scheme allows LLMs to address various graph queries with high efficacy, efficiency, and robustness, while reducing computational costs on large-scale graph tasks. Furthermore, we demonstrate the interpretability of our model using intrinsic attention weights and established explainers. Comprehensive evaluations across diverse graph reasoning and real-world tasks of node, link, and graph-levels highlight the superiority of our method, marking a significant advancement in the application of LLMs to graph understanding.

1 Introduction

Large Language Models (LLMs) (Vaswani et al., 2017; Devlin et al., 2018; Achiam et al., 2023; Chowdhery et al., 2023) have demonstrated impressive generative capabilities, revolutionizing multiple fields, including natural language processing (NLP), computer vision (Wang et al., 2024c; Parashar et al., 2024; Liu et al., 2024b), speech recognition (Fathullah et al., 2024), and cross-modal domains (Wu et al., 2023; Koh et al., 2024). Despite this widespread success, their application to graph tasks remains an emerging area of research (Chen et al., 2024c; Ren et al., 2024; Jin et al., 2023). Unlike linear text data, graph data presents unique challenges due to its non-Euclidean topologies and intricate structures (Jin et al., 2023), making it difficult for LLMs to process these complex relationships effectively. As a result, the adoption of LLMs in graph-centric tasks has been limited, with graph models such as Graph Neural Networks (GNNs) (Kipf & Welling, 2017; Gilmer et al., 2017; Wang et al., 2019; Iyer et al., 2021; 2022) continuing to be the state-of-the-art in this domain.

Applying LLMs to graph tasks presents two key challenges. Firstly, real-world graphs, such as molecules, often involve complex combinations of features and structures (Qin et al., 2023), such as atomic properties and the bonds between atoms. While LLMs excel at processing feature-based information due to their strong text comprehension abilities, they often falter with structural details (Hu et al., 2023). This limitation leads to their suboptimal performance even on simple graph tasks, such as identifying shortest paths (Guo et al., 2023; Wang et al., 2024a; Fatemi et al., 2023). Consequently, LLMs tend to perform well mainly on node-level tasks but struggle with more complex link and graph-level tasks, where understanding long-range structures is crucial (Liu et al., 2023; Wu et al., 2021). Secondly, representing graphs within LLMs poses significant scalability challenges (Zhao et al., 2023; Ye et al., 2023b). Encoding both feature and structural information for each graph node, as in molecular (Dwivedi et al., 2023), citation (Hu et al., 2020b), or knowledge graphs (Dettmers et al., 2018), often results in lengthy prompts. This dramatically increases computational complexity, as the attention mechanism in LLMs scales quadratically with input size, making the application of LLMs to large graph-based tasks computationally prohibitive and demanding specialized solutions. On the other hand, a key advantage of using LLMs for graph tasks is their capacity to process graphs in a human-comprehensible manner, accepting input as straightforward text descriptions. With a human-readable vocabulary, LLMs offer a natural advantage in interpretability over the opaque embeddings

utilized by GNNs (Binder et al., 2016; Longo et al., 2024; Achtibat et al., 2024). However, no prior work has focused on providing interpretable results that explain graph structures.

To address these challenges, we introduce Hierarchical Language Model for Graphs (HLM-G), a novel framework designed to enhance the graph structure comprehension capabilities of LLMs. Unlike conventional LLMs that apply self-attention across all tokens, HLM-G employs a two-block architecture, comprising a local block and a global block, each with specialized attention masking. This hierarchical structure enables the model to initially capture local information in the lower layers, followed by the integration of global-level information in the upper layers. Our approach not only enhances the model's understanding of graph structures but significantly reduces computational costs, making HLM-G more scalable for large-scale graph tasks. Furthermore, our hierarchical design exhibits increased robustness to variations in graph prompts. We also demonstrate the interpretability of our hierarchical language model with both model intrinsic weights and established explainers. Finally, we conduct comprehensive experiments across seven graph reasoning datasets and seven real-world datasets, encompassing citation networks, knowledge graphs, and molecular graphs. Our results validate HLM-G's ability to generalize effectively across node, link, and graph-level tasks, marking a significant advancement in the application of language models to graph-based tasks.

2 Background and Related Work

Problem Setup. We denote a graph as $G = (\boldsymbol{A}, \boldsymbol{X}, \boldsymbol{E})$, where $\boldsymbol{A} \in \mathbb{R}^{n \times n}$, $\boldsymbol{X} \in \mathbb{R}^{p \times n}$, and $\boldsymbol{E} \in \mathbb{R}^{q \times m}$ represent the adjacency, node feature, and edge feature matrices, respectively. Here, n, m, p, and q denote the numbers of nodes, edges, node features, and edge features, respectively. Building on these, we describe graph tasks in natural language. For each graph G_i, we first construct a sequence U_i that encapsulates the natural language descriptions of G_i covering $\boldsymbol{A}_i$, $\boldsymbol{X}_i$, and $\boldsymbol{E}_i$, coupled with a query Q_i describing the prediction task. Each task is also associated with a true label $y_i \in \mathcal{Y}$. This leads to a dataset of sequences $\boldsymbol{U} = \{(U_1, Q_1, y_1), (U_2, Q_2, y_2), \cdots, (U_N, Q_N, y_N)\}$, where each sequence $U_i = \{u_1, u_2, \cdots, u_{l_i}\}$ and all tokens u_i belong to a vocabulary $\mathcal{V}$.

LLM Inference Methods. Prompt engineering has been pivotal in adapting LLMs for a wide range of tasks (Sahoo et al., 2024a; Zhou et al., 2022). Early attempts in prompt engineering for graph tasks use structured representations like edge lists and adjacency matrices (Brandes et al., 2013; Zhao et al., 2023), but these methods struggle with graph structural reasoning tasks (Guo et al., 2023). NLGraph (Wang et al., 2024a) seeks to convert graph data into natural language prompts, yet fundamental graph operations remain challenging, even for small graphs. Studies suggest simpler prompts can be more effective, but overall improvements are still modest (Zhao et al., 2023; Fatemi et al., 2023; Sahoo et al., 2024b). Beyond prompt engineering, other approaches (Yao et al., 2024; Wang et al., 2022) involve exploring multiple reasoning paths and selecting the most confident one, offering marginal gains at the cost of increased inference time. LLMs continue to underperform compared to specialized graph models, indicating a significant gap (Hu et al., 2023). The limited success of LLMs on graphs has been partly attributed to their inability to construct coherent world models, often relying on pattern matching rather than genuine reasoning (Valmeekam et al., 2023; Stechly et al., 2024).

LLM Fine-Tuning Methods. Fine-tuning and instruction tuning have been investigated to address LLMs' limitations in graph reasoning tasks. Fine-tuning on graph-specific datasets has achieved limited success, with models still struggling to capture complex graph structures (Tang et al., 2023; Vafa et al., 2024). Instruction tuning, which aligns training objectives with graph reasoning tasks, has shown more promise (Wang et al., 2024b; Luo et al., 2024) by introducing a variety of related tasks during training, enabling LLMs to gain a deeper understanding of the graph domain. However, this approach is labor-intensive and continues to face challenges with large and dense graphs. Methods such as GraphWiz (Chen et al., 2024a) have further incorporated RL preference alignment (Rafailov et al., 2024), demonstrating some improvements but still struggling with dense graph structures. Furthermore, incorporating real-world graph features, such as node and edge features in citation networks, into LLMs remains an open challenge, indicating that more work is needed to adapt LLMs for graph tasks.

Hybrid GNN-LLM Methods. Hybrid models aim to leverage the complementary strengths of LLMs and GNNs, combining the textual understanding capabilities of LLMs with the graph-processing proficiency of GNNs. In these approaches, LLMs are often used to enhance graph representations by providing enriched feature descriptions, as demonstrated in models like GIANT (Chien et al., 2021) and LM-GNN (Ioannidis et al., 2022). Alternatively, other methods such as G-Retrieval (He et al., 2024), LLaGA (Chen et al., 2024b), and GraphLLM (Chai et al., 2023) incorporate graph models and employ LLMs as predictors to improve graph reasoning tasks. Despite their effectiveness, these hybrid models inherit certain limitations associated with GNNs, such as oversmoothing (Rusch et al., 2023), and require task-specific architecture designs (You et al., 2020), which involves distinct structures for node, link, and graph-level tasks. Additionally, these approaches face challenges in interpretability, as they often rely on opaque embeddings, unlike LLM-only methods which enables token-level linguistic interpretations. Such token-level interpretability is inherently more human-understandable and offers clearer insights into the decision-making process.

3 Hierarchical Language Model Design

In this section, we introduce our Hierarchical Language Model, designed to effectively capture both the structural and feature-based aspects of graphs. We begin by explaining how graph data can be transformed into natural language descriptions (Section 3.1). Following this, we describe the model's architecture, which is composed of a local block (Section 3.2) for learning local structural information, a pooling layer (Section 3.3) for integrating structural and feature information, and a global block (Section 3.4) for capturing global information. This hierarchical approach not only guides our model to better understand graph structures but also results in computational advantages.

3.1 Natural Language Descriptions of Graphs

Following prior works (Guo et al., 2023; Fatemi et al., 2023) that demonstrate the effectiveness of using simpler graph inputs for LLMs, we define a graph-to-text representation U to describe any graph task in natural language. For a graph G characterized by its adjacency matrix $\boldsymbol{A}$, node features $\boldsymbol{X}$, and edge attributes $\boldsymbol{E}$, we construct textual representations capturing both node feature and 1-hop structural information for each node v_i in G. These representations are divided into two components: the node feature annotation U_i^X and the node structure annotation U_i^{AE}.

Node Feature Annotation. Each node can be effectively described in natural language and presented as input to an LLM. The node feature annotation for a node v_i, denoted as U_i^X, is a natural language sequence that describes the attributes $\boldsymbol{X}_i$ of v_i over a predefined vocabulary $\mathcal{V}$. The template for U_i^X is as follows:

> U_i^X **:** Node <*i*> features: <feature_1>: <content_1>$\cdots$, <feature_p>: <content_p>.
> **E.g. 1 (Citation Network):** Node 97 features: Title: A Zero-Knowledge Revocable Credential Verification Protocol Using Attribute-Based Encryption; Abstract: We introduce a zero-knowledge credential verification protocol leveraging Ciphertext Policy Attribute-Based...
> **E.g. 2 (Molecule):** Node 10 features: Atomic Number: 7; Degree: 2; Formal charge: 5; Number of Hydrogens: 0; Radical electrons: 0; Hybridization: SP2; Aromatic: True; In Ring: False.

Node Structure Annotation. The node structure annotation U_i^{AE} captures the structural connections of node v_i within the graph G, including its connections to other nodes and the corresponding edge features. This serves as a textual representation of $\boldsymbol{A}$ and $\boldsymbol{E}$. Let $ne(i)_1, ne(i)_2, \ldots, ne(i)_k$ be the indices of v_i's 1-hop neighbors in G. The template for $U_{v_i}^{AE}$ is:

> $U_{v_i}^{AE}$ **:** Node <*i*> is connected to <*ne(i)*$_1$> with <*edge_feature*$_1$>, <*ne(i)*$_2$> with <*edge_feature*$_2$>, $\cdots$, and <*ne(i)*$_k$> with <*edge_feature*$_k$>.
> **E.g. 1 (Citation Network):** Node 20 is connected to nodes 10, 14, and 19.
> **E.g. 2 (Molecule):** Node 11 is connected to nodes 10 and 13 by a double bond,. . . and to node 27 by a conjugated double bond.

Task Query. We define a task-specific query Q to represent the prediction task in natural language. This query is tailored for each prediction scenario, as demonstrated below:

Q_G **:** What is the prediction for$\cdots$
E.g. 1: What is the shortest distance between nodes 0 and 1?
E.g. 2: Does the molecule inhibit HIV virus replication?

Graph Task Reformulation. Any graph-level task can be reformulated using a concatenation of all nodes' respective $U_{v_i}^X$ and $U_{v_i}^{AE}$ along with the task query Q. Formally, this representation is given by:

$$\begin{aligned} f(G) &= \text{concat}(U_G, Q_G) \\ &= \text{concat}(U_{v_1}^{AE}, U_{v_1}^X, \ldots, U_{v_n}^{AE}, U_{v_n}^X, Q_G), \end{aligned}$$

where $v_i \in G$ and $\text{concat}(\cdot)$ represents the sequence concatenation operation.

While the feature descriptions are generally standardized, there are multiple ways to describe the structural information of a graph. We explore various prompting strategies in Appendix F.2.

3.2 The Local Block

Since language models cannot inherently understand graphs in their natural structure, we introduce a local-to-global guidance approach, where the model first learns strong local features before capturing information at the global graph level. To implement this, we introduce a local block M_L that employs an intra-node attention masking mechanism. This mechanism ensures that, for each node v_i, the combined text sequence $(U_{v_i}^{AE}, U_{v_i}^X)$ is processed independently of other nodes, allowing the model to effectively capture node-specific structures and features. Given an input token sequence $H^l \in \mathbb{R}^{n \times d_k}$ at any transformer layer, where n is the total number of tokens across all nodes and d_k is the embedding dimension, we decompose this sequence into segments: $H^l = \{H_1, H_2, \ldots, H_N\}$, with each segment $H_i \in \mathbb{R}^{n_i \times d_k}$ representing the tokens associated with node v_i. The attention mechanism in the local block is then formulated as:

$$\text{Attention}^{(l)}(Q, K, V) = \text{Diag}\left(\text{Attention}^{(l)}(Q_1, K_1, V_1), \ldots, \text{Attention}^{(l)}(Q_N, K_N, V_N)\right),$$

where

$$\text{Attention}^{(l)}(Q_i, K_i, V_i) = \text{Softmax}\left(\frac{(\boldsymbol{W}_Q^{(l)} \boldsymbol{H}_i^{(l-1)})(\boldsymbol{W}_K^{(l)} \boldsymbol{H}_i^{(l-1)})^T}{\sqrt{d_k^{(l)}}}\right)(\boldsymbol{W}_V^{(l)} \boldsymbol{H}_i^{(l-1)}).$$

This block diagonal attention mechanism also provides several computational advantages. Let n_i^X and n_i^{AE} represent the number of tokens corresponding to the feature annotation U_i^X and structure annotation U_i^{AE} for node v_i, respectively. The total number of tokens n for the entire graph is given by $n = \sum n_i$, where $n_i = n_i^X + n_i^{AE}$. By employing this block diagonal attention mechanism, we achieve significant computational efficiency compared to traditional full attention approaches. In standard attention, the computational complexity is typically $\mathcal{O}\left((\sum n_i)^2\right)$, which scales quadratically with the total number of nodes, becoming increasingly expensive for larger graphs. In contrast, our block diagonal design reduces the complexity to $\mathcal{O}\left(\sum n_i^2\right)$, resulting in a linear scaling relative to the number of nodes. This improvement substantially enhances efficiency, especially for larger graph-based tasks, making our approach highly scalable.

3.3 Pooling Layer

To integrate structural and feature-based information extracted from the graph, we introduce a pooling mechanism. For each node v_i, we first derive local embeddings from the hidden states produced by the local block M_L. Specifically, the feature-based embedding is obtained as $\boldsymbol{z}_{v_i}^X = \frac{1}{n_i^X} \sum_{j=1}^{l_i} \boldsymbol{h}_j$, where $\boldsymbol{h}_j$ represents the hidden states corresponding to tokens from U_i^X. Similarly, the structure-based embedding $\boldsymbol{z}_{v_i}^{AE}$ is obtained from $U_{v_i}^{AE}$ using the same approach. Next, we combine these embeddings through a parameterized pooling

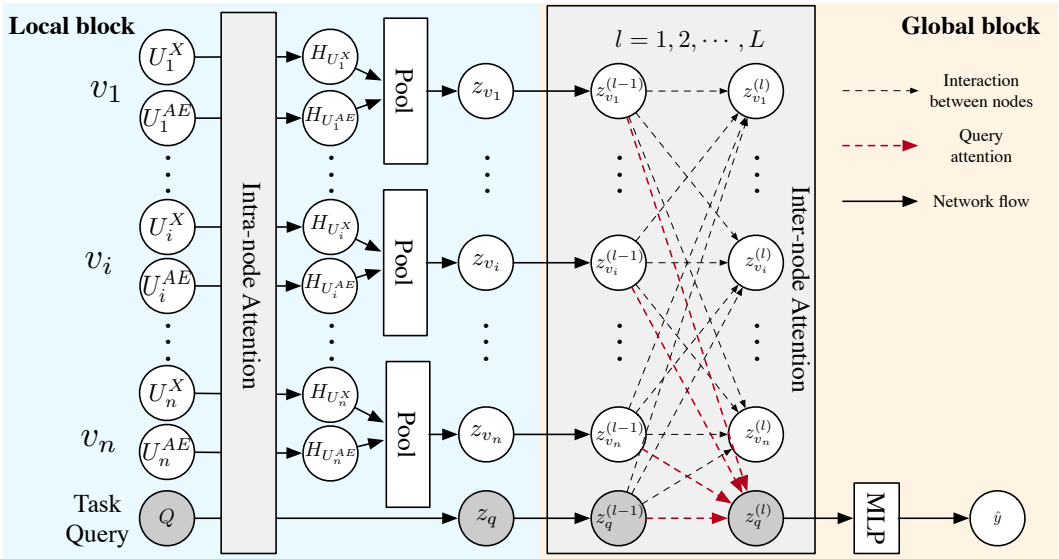

Figure 1: **Hierarchical Model Design**: Local Block employs intra-node attention to learn local node and structural features. Pooling layer combines these features and Global Block utilizes inter-node attention to capture higher-level interactions, enabling comprehensive graph understanding. The Hierarchical model design results in a model which is highly scalable and delivers robust performance across both structure reasoning tasks and real world graph prediction tasks. The model also supports dual interpretability: node-level interpretability through the Global Block and fine-grained token-level interpretability via the Local Block, making it not only powerful but also transparent in its predictions.

operation to produce the final embedding $\boldsymbol{z}_i$ for each node. Formally, given a sample U, the pooled embedding is defined as:

$$\boldsymbol{z}_i = \alpha \boldsymbol{z}_{v_i}^{AE} + (1-\alpha)\boldsymbol{z}_{v_i}^{X},$$

where $\alpha \in (0,1)$ is a trainable parameter that balances the contribution of structural ($\boldsymbol{z}_{v_i}^{AE}$) and feature ($\boldsymbol{z}_{v_i}^{X}$) information. A larger α emphasizes the structural properties in the final prediction, while a smaller α gives more weight to feature-based characteristics.

Our adaptive pooling mechanism allows our model to work for tasks requiring varying levels of structural and feature importance, such as link and graph-level tasks that demand greater structural emphasis and node-level tasks that rely more heavily on feature-based information. We ablate alternative pooling strategies and configurations, which are detailed in Appendix F.

3.4 The Global Block

To capture global-level interactions across the entire graph, we introduce the global block M_G, which leverages a multi-layer transformer architecture to model comprehensive structural relationships. The global block operates on top of the local embeddings derived from M_L, learning the higher-level interactions between nodes and enriching the representation with more nuanced graph-level information. Each layer comprises an attention mechanism followed by a feedforward layer. For any layer l, the embeddings are updated as:

$$\boldsymbol{Z}^{(l)} = \text{Softmax}\left(\frac{(\boldsymbol{W}_Q^{(l)}\boldsymbol{Z}^{(l-1)})(\boldsymbol{W}_K^{(l)}\boldsymbol{Z}^{(l-1)})^T}{\sqrt{d_k}}\right)(\boldsymbol{W}_V^{(l)}\boldsymbol{Z}^{(l-1)}),$$
$$\boldsymbol{Z}^{(0)} = [\boldsymbol{z}_{v_1}, \cdots, \boldsymbol{z}_{v_n}, \boldsymbol{z}_q],$$

where d_k is the dimensionality of the key vectors, and $\boldsymbol{W}_Q^{(l)}, \boldsymbol{W}_K^{(l)}, \boldsymbol{W}_V^{(l)}$ are the weight matrices. The input $\boldsymbol{Z}^{(0)}$ includes node embeddings $\boldsymbol{z}_{v_1}, \ldots, \boldsymbol{z}_{v_n}$ and the task-specific query embedding $\boldsymbol{z}_q$ from M_L. After

processing through L layers, the final embedding $\boldsymbol{z}_q^{(L)}$ is passed through a multilayer perceptron (MLP) to generate the prediction:

$$\hat{y} = \text{argmax}\,\text{MLP}(\boldsymbol{z}_q^{(L)}), \quad \text{where } \boldsymbol{z}_q^{(L)} = \boldsymbol{Z}_{:,n+1}^{(L)},$$

with $\hat{y}$ representing the predicted class label. The training objective is to minimize cross-entropy loss:

$$\{\theta_L, \theta_G, \psi\}^* = \underset{\theta_L,\theta_G,\psi}{\text{argmin}}\, \mathbb{E}_{(U,y)\sim\boldsymbol{U}} \left[\ell(y; \text{MLP}(M_G(M_L(U))))\right],$$

where y is the ground truth label, and θ_L, θ_G, ψ represent the trainable parameters of M_L, M_G, and the MLP, respectively.

4 Experiments

In this section, we conduct experiments to investigate four specific research questions (RQs) to assess the effectiveness of our model on graph tasks: **RQ1**: Can our model accurately understand the underlying structures and maintain robust performance across different graph reasoning datasets? **RQ2**: Does our approach enhance interpretability performance and produce intrinsic interpretable results? **RQ3**: Can the proposed method handle complex real-world datasets with diverse node or edge features? **RQ4**: Does the proposed method work well across all node, link and graph level tasks?

4.1 Structure Understanding Capabilities over Graph Reasoning Datasets

To answer RQ1, we aim to validate whether our model can process graph structure information by conducting the following experiments on graph reasoning datasets.

Datasets. First, following Wang et al. (2024a), we create a synthetic dataset consisting of seven graph reasoning tasks to assess the structural reasoning capabilities of our model. These datasets were constructed by a Random Graph Generator capable of generating graphs with up to 40 nodes and 700+ edges. Further information on these datasets is provided in Appendix C.1.1.

Baselines. We compare our method against both GNN-based and LLM-based approaches. On the GNN side, our comparisons include models such as GCN (Kipf & Welling, 2017), GAT (Veličković et al., 2017), and the more expressive GIN (Xu et al., 2018), as well as the graph transformer model, GTN (Yun et al., 2019). For LLMs, our inference-only methods include Zero-Shot (Huang et al., 2023), Chain of Thought (CoT) (Wei et al., 2023), CoT Self Consistency (CoT-SC) (Wang et al., 2022), and Natural Language Graph (NLGraph) (Wang et al., 2024a) prompting. Additionally, fine-tuning baselines such as BERT (Devlin et al., 2019) and Lora-Trained (Hu et al., 2021) Llama 3 are used for direct comparisons. We include GraphWiz (Chen et al., 2024a) as a representative of instruction tuning. The GraphToken (Perozzi et al., 2024) method, which utilizes a GNN encoder to fine-tune a frozen LLM, is also compared. Detailed information on our experimental configurations and hyperparameters can be found in Appendix C.2. For LLMs, we use Llama-3 8B (Dubey et al., 2024) as the primary backbone.

4.1.1 Quantitative Comparisons.

Our method demonstrates state-of-the-art performance across all graph reasoning datasets, significantly outperforming all baselines, both GNN and LLM-based models. Notably, GNNs such as GIN, despite their theoretically strong expressiveness as validated by the WL-1 test (Huang & Villar, 2021), struggle with graph-level tasks, failing to match the comprehensive understanding offered by our model. Prompt engineering approaches, like CoT and NLGraph and exploration based approaches like CoT-SC do not yield substantial improvements in performance, particularly on tasks like shortest distance that demand a deeper comprehension of the graph structure. GraphToken, a hybrid GNN-LLM approach shows limited gains, indicating that using GNN-augmented LLMs is insufficient for achieving top performance in graph tasks.

While instruction-tuned models like GraphWiz exhibit better results on smaller graphs, they face significant challenges with larger and denser graphs. Notably, their performance is strong on graphs with up to 100 edges, reaching accuracies of 93% and 84% for the reachable and edge count tasks, respectively. However, this

Table 1: **Graph reasoning performance comparisons.** This table showcases our HLM-G model against 11 baselines across 7 graph reasoning datasets. Our method not only achieves state-of-the-art performance among all LLMs but also outperforms GNNs on 6 out of 7 tasks. The table details the performance of each method in terms of accuracy across various node, link, and graph-level tasks, underlining the superior capability of our HLM-G model in handling complex graph reasoning challenges.

Type	**Method**	**Node Degree**	**Edge Existence**	**Shortest Distance**	**Reachable**	**Cycle**	**Edge Count**	**Components**
	Task level	Node	Link	Link	Link	Graph	Graph	Graph
	# Classes	39	2	6	2	2	70	38
GNN	**GCN**	7.2±1.61	66.5±1.15	40.5±2.13	87.4±0.99	69.1±0.73	3.8±0.55	8.1±1.94
	GIN	97.7±0.48	94.7±0.56	**96.3±0.16**	**99.9**±0.13	**99.9±0.04**	65.5±2.35	68.8±0.8
	GTN	4.97±0.48	50.0±0.48	18.5±1.87	53.3±0.67	50.4±2.3	4.7±0.18	25.6±0.87
LLM-inference	**Zero Shot**	15.9±0.00	40.8±0.00	22.3±0.00	34.1±0.00	46.4±0.00	4.4±0.00	1.8±0.00
	COT	37.4±0.00	67.2±0.00	22.8±0.00	34.6±0.00	23.8±0.00	4.1±0.00	4.0±0.00
	COT-SC	37.9±0.00	69.9±0.00	24.3±0.00	41.8±0.00	24.8±0.00	7.4±0.00	4.3±0.00
	NLGraph	20.4±0.00	49.3±0.00	13.2±0.00	32.4±0.00	47.7±0.00	0.37±0.00	0.5±0.00
Hybrid GNN-LLM	**GraphToken**	22.4±2.30	64.7±0.90	54.7±1.34	54.6±2.89	73.4±1.85	7.8±0.31	5.2±0.09
LLM-finetuning	**BERT**	21.7±1.39	55.9±2.41	61.6±1.34	76.0±0.56	91.4±0.31	97.2±0.26	29.2±0.59
	Llama 3	41.1±0.13	92.6±1.01	48.3±0.34	84.7±0.69	89.8±0.98	29.1±3.16	9.2±1.44
	Graphwiz	29.6±1.31	87.7±1.11	47.1±1.77	75.9±1.06	84.1±0.09	37.8±3.10	19.9±3.88
	HLM-G (Ours)	**99.9±0.04**	**100±0.00**	84.6±0.43	**99.9±0.07**	**99.9±0.06**	**98.6±0.03**	**94.2±0.21**

accuracy drops sharply to 76% and 38% when the graphs become denser, with up to 700+ edges, as shown in Table 1. Our model remains highly effective in these dense scenarios, maintaining near-perfect accuracies across all tasks, demonstrating its robustness against graph complexity and density. Fine tuning a similar sized BERT and even 80X larger models like Llama-3 is unable to outperform our architecture, underscoring the fact that our design is better suited for graph based tasks than the traditional design.

4.1.2 Evaluation of Model Robustness.

A critical question emerges from the quantitative comparisons: *Do language models truly understand graph structures, or do they rely on pattern-matching?* To investigate this, we conducted a robustness evaluation by systematically shuffling the node indices of each graph using a permutation matrix P. Unlike GNNs, which are inherently invariant to changes in node indexing due to their symmetrical message-passing framework, LLMs may exhibit sensitivity to even slight alterations in node token representations, potentially leading to inconsistent predictions for the same graph described differently. This issue highlights a significant shortcoming of LLMs in graph-based tasks.

In this experiment, we applied the permutation matrix P 10 times to each graph, generating modified adjacency matrices $\boldsymbol{A}^t = P\boldsymbol{A}^{t-1}P^T$ at each iteration t. This process preserves the overall graph structure while changing the node indices, allowing us to evaluate whether the model's predictions remain consistent under different representations.

The results, presented in Table 2, highlight a stark difference between traditional LLM-based models and our proposed HLM-G model. NLGraph's performance dropped significantly, indicating that prompt engineering is not robust. Similarly, we observed that fine-tuned LLMs, such as Llama 3 and BERT, exhibited performance drops of up to 21% and 71%, respectively, on the Node Degree task. This highlights their high sensitivity to changes in node tokens and suggests a reliance on pattern recognition rather than a true comprehension of the underlying graph structure. Instruction tuning does not seem to provide robustness as Graphwiz also shows similar sensitivity as finetuned Llama 3. In contrast, our HLM-G model displays exceptional robustness, with minimal performance drops (e.g., a mere 6.1% drop on the Shortest Distance task and 0.0% on the Node Degree task). These findings underscore a crucial advantage of our HLM-G, while conventional LLMs struggle with variations in graph representation, our model remains robust, reinforcing its suitability for real-world graph tasks where representations might vary but the underlying structure remains unchanged.

4.2 Interpretability Comparisons

Having established the performance and robustness of our model, we now delve into analyzing its interpretability—specifically, its ability to accurately identify and prioritize the most critical structural elements

Table 2: **Structural Robustness Assessment.** This table displays the accuracy drop observed over 10 permutations for each task. Lower performance drop (↓) indicates less sensitivity to node description positions, highlighting the model's ability to learn graph structure effectively.

Method	Node Degree(↓)	Edge Existence(↓)	Shortest Distance(↓)	Reachable(↓)	Cycle(↓)	Edge Count(↓)	Components(↓)
NLGraph	46.1	38.1	56.6	44.1	49.4	71.6	71.3
BERT	71.4	11.0	46.2	14.3	9.4	7.8	62.8
LLaMA 3	21.5	11.9	28.9	8.6	15.9	44.8	62.2
GraphWiz	18.6	23.5	32.1	15.2	26.9	38.3	42.0
HLM-G (our method)	**0.0**	**0.0**	**6.1**	**0.8**	**0.1**	**3.0**	**10.2**

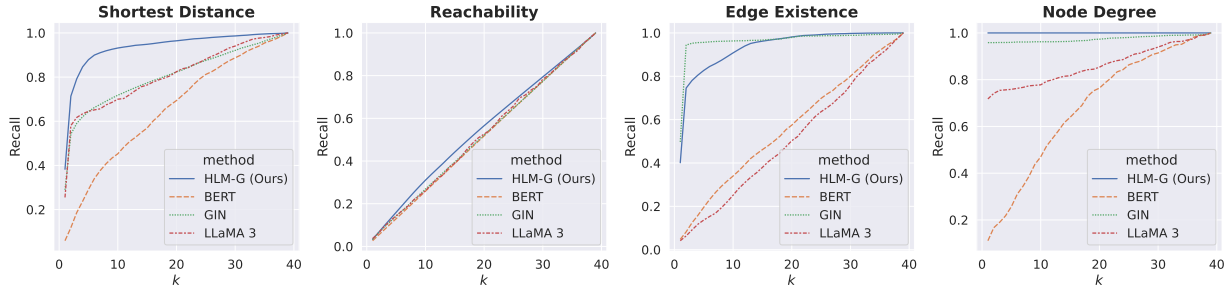

Figure 2: **Explainer Based Interpretation Comparisons.** This figure illustrates the interpretability performance of BERT, GIN, and our method on 4 graph reasoning datasets with reasoning ground truths. k indicates the k most important nodes that interpreted by the model are selected.

within graph reasoning tasks, thus addressing RQ2. Interpretability serves as a vital criterion in evaluating whether a model is capable of comprehending graph structures rather than just fitting patterns. For this purpose, we utilize four graph reasoning datasets that offer explicit ground truths regarding which nodes are genuinely important for a given graph task. For example, in the shortest distance task, the ground truth consists of nodes that lie along the shortest path between two specified nodes. More details about these ground truths are provided in Appendix E.1. We compare the true structure understanding capabilities of four finetuned models from Table 1: Llama-3, BERT, GIN and HLM-G.

To measure interpretability, each model is expected to generate an ordered set $\boldsymbol{r} = \{r_1, \ldots, r_n\}$ for a graph with n nodes, ranking them from the most to the least significant, based on the model's internal focus and reasoning. The quality of a model's interpretation is then evaluated by how effectively it identifies the nodes that align with the ground truths. Ideally, a model with true structural comprehension should consistently rank ground truth nodes higher, indicating that it genuinely understands the critical elements of the graph structure. Using established explainers, we first reveal the extent to which our approach successfully captures and prioritizes the essential graph components. We then introduce the intrinsic interpretability mechanism built into our model, demonstrating its ability to provide ready made interpretations.

4.2.1 Explainer-based Interpretation

To objectively compare the interpretability performance across different models, we leverage established explainability techniques such as Saliency (Simonyan et al., 2013), Input x Gradient (Shrikumar et al., 2016), DeepLIFT (Shrikumar et al., 2017), and GNNExplainer (Ying et al., 2019). This approach allows us to assess how well each model can identify and rank important graph elements, providing insight into the structural modeling capabilities of these models. More details on this strategy, referred to as "explanations as interpretations", are outlined in Appendix E.2.

Setup. To quantify interpretability, we use a Recall@k metric, which measures how effectively a model identifies the nodes that correspond to ground truths. Given a set of ground truth nodes $\boldsymbol{r}^{gt}$ and the set of top-k nodes identified by the model $\boldsymbol{r}^k = \{r_1, \ldots, r_k\}$, we calculate Recall@$k$ as $\text{Recall}(k) = \frac{|\boldsymbol{r}^k \cap \boldsymbol{r}^{gt}|}{|\boldsymbol{r}^{gt}|}$, where $|\cdot|$ represents the cardinality of the set and $\cap$ denotes the intersection. As shown in Figure 2, we evaluate

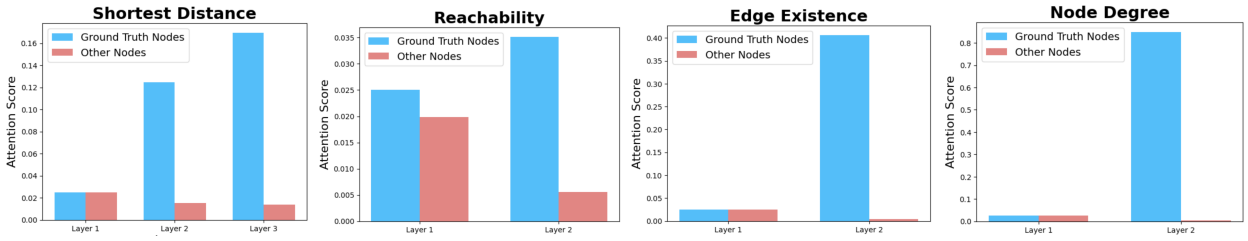

Figure 3: **Layer-by-Layer Attention Interpretation.** This figure compares the mean attention scores for relevant nodes with irrelevant nodes across each layer of the model in 4 graph reasoning tasks. The increased scores in higher layers emphasizes the model's capability to learn larger scale structure information and identify relevant graph nodes effectively.

each model's performance by plotting the recall curve for $k \in \{1, 2, \ldots, n\}$, where n represents the total number of nodes in the graph. Ideally, a model with a strong understanding of graph structure will have high recall values across different values of k, indicating that it consistently identifies the most important nodes.

Results and Analysis. Figure 2 presents the interpretability results for the four models across the four graph reasoning datasets. Our HLM-G model demonstrates superior interpretability, particularly as k increases, indicating a higher proficiency in pinpointing the most relevant nodes for each task. While GIN performs adequately on tasks requiring simpler one-hop reasoning, such as Edge Existence and Node Degree, it struggles with more complex, multi-hop reasoning tasks like Shortest Distance and Reachability. In contrast, BERT and LLaMA consistently fail to identify relevant structural features, reflecting their limited capability to capture intricate graph patterns. Directly fine-tuning LLMs has not led to significant improvements in these cases. Although Llama 3 outperforms BERT on three out of four tasks, it still does not reach the performance level of GIN or our model. Our model, in fact, excels across all tasks, even those involving multi-hop reasoning, which further confirms its strong understanding of graph structures beyond simple pattern matching.

4.2.2 Intrinsic Attention Interpretation

A key strength of our model design is its inherent interpretability, distinguishing it from existing methods. The local embedding matrix $\boldsymbol{Z}^{(0)}$ in the local block captures 1-hop subgraph information, where each $\boldsymbol{z}_{v_i} \in \boldsymbol{Z}^{(0)}$ represents the 1-hop ego-graph centered around node v_i. As the transformer layers progress in the global block, they progressively integrate this localized information to capture broader global structures within the graph. This means that embeddings in the higher layers reflect increasingly comprehensive structural details. The attention weights associated with the task query node in the global block provide a direct interpretation of the contribution of each node's structural information to the final prediction, effectively acting as importance scores for each node. This allows for a direct, interpretable insight into how the model makes its decisions.

To illustrate this, we analyze the mean attention scores across all layers, as shown in Figure 3. As we move to higher layers, the attention scores for ground truth nodes increase, while scores for other nodes decrease. This pattern directly confirms that our model effectively focuses on the most important nodes, demonstrating its ability to capture larger-scale structural information. These attention-based interpretations offer clear insights into the model's decision-making process without requiring additional explanation techniques.

4.3 Graph Learning Ability on Real-World Datasets.

Datasets. To answer the RQ3 and RQ4, we curated seven graph datasets widely recognized in the graph learning community, varying in scale, domains, and task types. We adopt Arxiv (Hu et al., 2020b), Cora (Bojchevski & Günnemann, 2018), and Pubmed (Sen et al., 2008) for node-level tasks; Pubmed, WN18RR (Bordes et al., 2013), and FB15k-237 (Bordes et al., 2013) for link-level tasks; and molhiv (Hu et al., 2020a) for graph-level tasks. More dataset details are discussed in Table 7.

Table 3: **Node-level comparisons.** This table compares our method with 7 baselines on node-level tasks. Types of methods are grouped based on their underlying approaches. All results are reported as averaged Accuracy with standard deviations across 3 random runs. The best and second-best results are highlighted in **bold** and underline respectively.

	GNN			GT	LLM-inference		LLM-finetuning	
Dataset	GCN	GAT	GraphSage	Graphormer	Zero-shot	Few-shot	InstructGLM	HLM-G (Ours)
arxiv	71.74±0.29	73.65±0.11	71.49±0.27	72.81±0.23	74.0±0.00	72.9±0.00	**75.70±0.12**	74.81±0.07
Pubmed	88.9±0.32	83.28±0.12	86.85±0.11	88.24±1.50	88.6±0.00	85.0±0.00	93.84±0.25	**94.62±0.13**
Cora	87.78±0.96	76.70±0.42	86.58±0.26	80.41±0.30	66.1±0.00	65.1±0.00	87.08±0.32	**88.5±0.43**

Table 4: **Link-level comparisons.** This table demonstrates the comparisons between our method and 4 baselines on link-level tasks. We evaluate Pubmed by ROC-AUC, others by Accuracy.

	GNN		GNN-LLM	LLM-finetuning	
Dataset	GCN	GIN	OFA	InstructGLM	HLM-G (Ours)
Pubmed	91.10±0.50	67.88±5.45	98.21±0.02	95.92±1.91	**98.47±0.18**
FB15k-237	74.20±1.10	70.70±1.80	95.54±0.06	64.39±0.98	**95.71±0.13**
WN18RR	67.40±2.40	57.30±3.40	96.91±0.11	63.8±1.5	**98.09±0.54**

Table 5: **Graph-level comparisons.** This table demonstrates the comparisons between our method and 6 baselines on graph-level task. We evaluate molhiv by ROC-AUC.

	GNN			GT	GNN-LLM	LLM-finetuning	
Dataset	GCN	GAT	GIN	GTN	Momu	Mamba	HLM-G (Ours)
molhiv	75.49±1.63	74.45±1.53	76.26±1.41	**77.67±1.49**	75.92±0.85	74.23±0.12	76.49±0.33

Baselines. We compare with traditional GNNs including GCN (Kipf & Welling, 2017), GAT (Veličković et al., 2017), GIN (Xu et al., 2018) and GraphSage (Hamilton et al., 2017). For graph transformer-based baseline we include GTN (Yun et al., 2019) and Graphormer (Ying et al., 2021). For LLMs, we compare Zero-shot and Few-shot performance using GPT 3.5 (Ye et al., 2023a) for node-level tasks, and Llama-2-7B finetuned InstructGLM (Ye et al., 2023b) for both node and link-level tasks. For the graph-level task, we compare with a GNN-LLM hybrid model Momu (Su et al., 2022) for molecular graphs. Note that we use Mamba (Gu & Dao, 2023) as a baseline for graph-level task as no Transformer-based LLM is computationally feasible for training on real-world graph-level tasks. OFA (Liu et al., 2024a), a hybrid GNN-LLM model, is also selected as a baseline due to its strong performance on link-level tasks.

Quantitative Results. As demonstrated in Tables 3, 4, and 5, our method consistently delivers competitive performance across node, link, and graph-level tasks. Compared to traditional GNNs, our model surpasses their performance for both node and link-level tasks with large margins. In comparison to hybrid GNN-LLM methods, our model notably outperforms the recently developed LLM-equipped OFA, on link-level tasks where OFA is considered especially strong. Furthermore, our model consistently perform favorably against LLM instruction tuning approach - InstructGLM across link level tasks. Although graph transformers perform slightly better in the graph-level task because of their specialized encodings for graph-level tasks, our model produces much higher performance than them in node-level tasks. It is noteworthy that while LLM-only models excel in node-level tasks, they experience a marked decline in performance on link-level tasks, validated their limitations in processing structural information mentioned in Section 2. A crucial factor in our model's adaptability across all task levels is our pooling parameter α discussed in detail in Appendix F.1. This enables our model to adjust its reliance on structural or feature-based information, thereby allowing it to generalize

well across all levels. Our model's ability to dynamically adjust α provides a significant advantage, making it more versatile and capable of handling a wide range of graph-centric tasks.

Overall, our experiments highlight our model's computational efficiency (Appendix D.3), ability to process structural information, interpretability, and effectiveness across diverse tasks. For additional experiments and ablation studies, please refer to Appendix D and Appendix F respectively.

5 Conclusions and Discussions

In this paper, we introduce a novel Hierarchical Language Model to tackle the complexities of non-Euclidean structures commonly found in graphs. While language models excel in text-centric applications, they often struggle with the intricate structures of graph data, leading to significant performance and computational challenges. Additionally, the context length, which involves the natural language description of a graph, can become enormous for real-world datasets, rendering them ineffective for graphs. Our method sets itself apart by designing a hierarchical architecture to process the graph structure and enhance computational efficiency and interpretability. We show that our model yields promising results in graph reasoning tasks as well as robust and consistent performance on real-world datasets, outperforming most models designed for similar purposes.

This work paves the way for future research in language models for graph learning, establishing a solid foundation for innovation and providing valuable insights into this emerging field. Our findings significantly narrow the gap between conventional language models and graph tasks, expanding potential applications and improving the effectiveness of language models in handling structured data. We hope this work can shed light on the future direction of LLM-based graph learning.

References

Josh Achiam, Steven Adler, Sandhini Agarwal, Lama Ahmad, Ilge Akkaya, Florencia Leoni Aleman, Diogo Almeida, Janko Altenschmidt, Sam Altman, Shyamal Anadkat, et al. GPT-4 technical report. *arXiv preprint arXiv:2303.08774*, 2023.

Reduan Achtibat, Sayed Mohammad Vakilzadeh Hatefi, Maximilian Dreyer, Aakriti Jain, Thomas Wiegand, Sebastian Lapuschkin, and Wojciech Samek. Attnlrp: attention-aware layer-wise relevance propagation for transformers. *arXiv preprint arXiv:2402.05602*, 2024.

Alexander Binder, Grégoire Montavon, Sebastian Lapuschkin, Klaus-Robert Müller, and Wojciech Samek. Layer-wise relevance propagation for neural networks with local renormalization layers. In *Artificial Neural Networks and Machine Learning–ICANN 2016: 25th International Conference on Artificial Neural Networks, Barcelona, Spain, September 6-9, 2016, Proceedings, Part II 25*, pp. 63–71. Springer, 2016.

Mitchell Black, Zhengchao Wan, Gal Mishne, Amir Nayyeri, and Yusu Wang. Comparing graph transformers via positional encodings. *arXiv preprint arXiv:2402.14202*, 2024.

Aleksandar Bojchevski and Stephan Günnemann. Deep gaussian embedding of graphs: Unsupervised inductive learning via ranking. In *International Conference on Learning Representations*, 2018. URL `https://openreview.net/forum?id=r1ZdKJ-0W`.

Antoine Bordes, Nicolas Usunier, Alberto Garcia-Duran, Jason Weston, and Oksana Yakhnenko. Translating embeddings for modeling multi-relational data. *Advances in neural information processing systems*, 26, 2013.

Ulrik Brandes, Markus Eiglsperger, Jürgen Lerner, and Christian Pich. Graph markup language (graphml). In *Handbook of Graph Drawing and Visualization*, 2013. URL `https://api.semanticscholar.org/CorpusID:142947`.

Ziwei Chai, Tianjie Zhang, Liang Wu, Kaiqiao Han, Xiaohai Hu, Xuanwen Huang, and Yang Yang. Graphllm: Boosting graph reasoning ability of large language model. *arXiv preprint arXiv:2310.05845*, 2023.

Nuo Chen, Yuhan Li, Jianheng Tang, and Jia Li. Graphwiz: An instruction-following language model for graph problems. *arXiv preprint arXiv:2402.16029*, 2024a.

Runjin Chen, Tong Zhao, Ajay Jaiswal, Neil Shah, and Zhangyang Wang. Llaga: Large language and graph assistant. *arXiv preprint arXiv:2402.08170*, 2024b.

Zhikai Chen, Haitao Mao, Hang Li, Wei Jin, Hongzhi Wen, Xiaochi Wei, Shuaiqiang Wang, Dawei Yin, Wenqi Fan, Hui Liu, et al. Exploring the potential of large language models (llms) in learning on graphs. *ACM SIGKDD Explorations Newsletter*, 25(2):42–61, 2024c.

Eli Chien, Wei-Cheng Chang, Cho-Jui Hsieh, Hsiang-Fu Yu, Jiong Zhang, Olgica Milenkovic, and Inderjit S Dhillon. Node feature extraction by self-supervised multi-scale neighborhood prediction. *arXiv preprint arXiv:2111.00064*, 2021.

Aakanksha Chowdhery, Sharan Narang, Jacob Devlin, Maarten Bosma, Gaurav Mishra, Adam Roberts, Paul Barham, Hyung Won Chung, Charles Sutton, Sebastian Gehrmann, et al. PaLM: Scaling language modeling with pathways. *Journal of Machine Learning Research*, 24(240):1–113, 2023.

Tim Dettmers, Pasquale Minervini, Pontus Stenetorp, and Sebastian Riedel. Convolutional 2d knowledge graph embeddings. In *Proceedings of the AAAI conference on artificial intelligence*, volume 32, 2018.

Jacob Devlin, Ming-Wei Chang, Kenton Lee, and Kristina Toutanova. Bert: Pre-training of deep bidirectional transformers for language understanding. *arXiv preprint arXiv:1810.04805*, 2018.

Jacob Devlin, Ming-Wei Chang, Kenton Lee, and Kristina Toutanova. Bert: Pre-training of deep bidirectional transformers for language understanding, 2019.

Abhimanyu Dubey, Abhinav Jauhri, Abhinav Pandey, Abhishek Kadian, Ahmad Al-Dahle, Aiesha Letman, Akhil Mathur, Alan Schelten, Amy Yang, Angela Fan, et al. The llama 3 herd of models. *arXiv preprint arXiv:2407.21783*, 2024.

Vijay Prakash Dwivedi, Anh Tuan Luu, Thomas Laurent, Yoshua Bengio, and Xavier Bresson. Graph neural networks with learnable structural and positional representations, 2022.

Vijay Prakash Dwivedi, Chaitanya K Joshi, Anh Tuan Luu, Thomas Laurent, Yoshua Bengio, and Xavier Bresson. Benchmarking graph neural networks. *Journal of Machine Learning Research*, 24(43):1–48, 2023.

Bahare Fatemi, Jonathan Halcrow, and Bryan Perozzi. Talk like a graph: Encoding graphs for large language models. *arXiv preprint arXiv:2310.04560*, 2023.

Yassir Fathullah, Chunyang Wu, Egor Lakomkin, Junteng Jia, Yuan Shangguan, Ke Li, Jinxi Guo, Wenhan Xiong, Jay Mahadeokar, Ozlem Kalinli, et al. Prompting large language models with speech recognition abilities. In *ICASSP 2024-2024 IEEE International Conference on Acoustics, Speech and Signal Processing (ICASSP)*, pp. 13351–13355. IEEE, 2024.

Matthias Fey and Jan Eric Lenssen. Fast graph representation learning with pytorch geometric, 2019.

Justin Gilmer, Samuel S Schoenholz, Patrick F Riley, Oriol Vinyals, and George E Dahl. Neural message passing for quantum chemistry. In *International conference on machine learning*, pp. 1263–1272. PMLR, 2017.

Albert Gu and Tri Dao. Mamba: Linear-time sequence modeling with selective state spaces. *arXiv preprint arXiv:2312.00752*, 2023.

Shurui Gui, Hao Yuan, Jie Wang, Qicheng Lao, Kang Li, and Shuiwang Ji. FlowX: Towards explainable graph neural networks via message flows. *IEEE Transactions on Pattern Analysis and Machine Intelligence*, pp. 1–12, 2023. doi: 10.1109/TPAMI.2023.3347470.

Jiayan Guo, Lun Du, and Hengyu Liu. Gpt4graph: Can large language models understand graph structured data? an empirical evaluation and benchmarking. *arXiv preprint arXiv:2305.15066*, 2023.

Will Hamilton, Zhitao Ying, and Jure Leskovec. Inductive representation learning on large graphs. *Advances in neural information processing systems*, 30, 2017.

Xiaoxin He, Yijun Tian, Yifei Sun, Nitesh V Chawla, Thomas Laurent, Yann LeCun, Xavier Bresson, and Bryan Hooi. G-retriever: Retrieval-augmented generation for textual graph understanding and question answering. *arXiv preprint arXiv:2402.07630*, 2024.

Edward J Hu, Yelong Shen, Phillip Wallis, Zeyuan Allen-Zhu, Yuanzhi Li, Shean Wang, Lu Wang, and Weizhu Chen. Lora: Low-rank adaptation of large language models. *arXiv preprint arXiv:2106.09685*, 2021.

Weihua Hu, Matthias Fey, Marinka Zitnik, Yuxiao Dong, Hongyu Ren, Bowen Liu, Michele Catasta, and Jure Leskovec. Open graph benchmark: Datasets for machine learning on graphs. In Hugo Larochelle, Marc Aurelio Ranzato, Raia Hadsell, Maria-Florina Balcan, and Hsuan-Tien Lin (eds.), *Advances in Neural Information Processing Systems 33: Annual Conference on Neural Information Processing Systems 2020, NeurIPS 2020, December 6-12, 2020, virtual*, 2020a. URL `https://proceedings.neurips.cc/paper/2020/hash/fb60d411a5c5b72b2e7d3527cfc84fd0-Abstract.html`.

Weihua Hu, Matthias Fey, Marinka Zitnik, Yuxiao Dong, Hongyu Ren, Bowen Liu, Michele Catasta, and Jure Leskovec. Open graph benchmark: Datasets for machine learning on graphs. *Advances in neural information processing systems*, 33:22118–22133, 2020b.

Yuntong Hu, Zheng Zhang, and Liang Zhao. Beyond text: A deep dive into large language models' ability on understanding graph data. *arXiv preprint arXiv:2310.04944*, 2023.

Jin Huang, Xingjian Zhang, Qiaozhu Mei, and Jiaqi Ma. Can llms effectively leverage graph structural information: when and why. *arXiv preprint arXiv:2309.16595*, 2023.

Ningyuan Teresa Huang and Soledad Villar. A short tutorial on the weisfeiler-lehman test and its variants. In *ICASSP 2021-2021 IEEE International Conference on Acoustics, Speech and Signal Processing (ICASSP)*, pp. 8533–8537. IEEE, 2021.

Qian Huang, Hongyu Ren, Peng Chen, Gregor Kržmanc, Daniel Zeng, Percy S Liang, and Jure Leskovec. Prodigy: Enabling in-context learning over graphs. *Advances in Neural Information Processing Systems*, 36, 2024.

Vassilis N Ioannidis, Xiang Song, Da Zheng, Houyu Zhang, Jun Ma, Yi Xu, Belinda Zeng, Trishul Chilimbi, and George Karypis. Efficient and effective training of language and graph neural network models. *arXiv preprint arXiv:2206.10781*, 2022.

Roshni G Iyer, Wei Wang, and Yizhou Sun. Bi-level attention graph neural networks. In *2021 IEEE International Conference on Data Mining (ICDM)*, pp. 1126–1131. IEEE, 2021.

Roshni G Iyer, Thuy Vu, Alessandro Moschitti, and Yizhou Sun. Question-answer sentence graph for joint modeling answer selection. *arXiv preprint arXiv:2203.03549*, 2022.

Bowen Jin, Gang Liu, Chi Han, Meng Jiang, Heng Ji, and Jiawei Han. Large language models on graphs: A comprehensive survey. *arXiv preprint arXiv:2312.02783*, 2023.

Diederik P Kingma and Jimmy Ba. Adam: A method for stochastic optimization. *arXiv preprint arXiv:1412.6980*, 2014.

Thomas N. Kipf and Max Welling. Semi-supervised classification with graph convolutional networks, 2017.

Jing Yu Koh, Daniel Fried, and Russ R Salakhutdinov. Generating images with multimodal language models. *Advances in Neural Information Processing Systems*, 36, 2024.

Xiang Lisa Li and Percy Liang. Prefix-tuning: Optimizing continuous prompts for generation, 2021.

Hao Liu, Jiarui Feng, Lecheng Kong, Ningyue Liang, Dacheng Tao, Yixin Chen, and Muhan Zhang. One for all: Towards training one graph model for all classification tasks. *arXiv preprint arXiv:2310.00149*, 2023.

Hao Liu, Jiarui Feng, Lecheng Kong, Ningyue Liang, Dacheng Tao, Yixin Chen, and Muhan Zhang. One for all: Towards training one graph model for all classification tasks. In *The Twelfth International Conference on Learning Representations*, 2024a. URL `https://openreview.net/forum?id=4IT2pgc9v6`.

Haotian Liu, Chunyuan Li, Qingyang Wu, and Yong Jae Lee. Visual instruction tuning. *Advances in neural information processing systems*, 36, 2024b.

Meng Liu, Hongyang Gao, and Shuiwang Ji. Towards deeper graph neural networks. In *Proceedings of the 26th ACM SIGKDD International Conference on Knowledge Discovery & Data Mining*, KDD '20. ACM, August 2020. doi: 10.1145/3394486.3403076. URL `http://dx.doi.org/10.1145/3394486.3403076`.

Luca Longo, Mario Brcic, Federico Cabitza, Jaesik Choi, Roberto Confalonieri, Javier Del Ser, Riccardo Guidotti, Yoichi Hayashi, Francisco Herrera, Andreas Holzinger, et al. Explainable artificial intelligence (xai) 2.0: A manifesto of open challenges and interdisciplinary research directions. *Information Fusion*, 106:102301, 2024.

Zihan Luo, Xiran Song, Hong Huang, Jianxun Lian, Chenhao Zhang, Jinqi Jiang, Xing Xie, and Hai Jin. Graphinstruct: Empowering large language models with graph understanding and reasoning capability. *arXiv preprint arXiv:2403.04483*, 2024.

Shubham Parashar, Zhiqiu Lin, Tian Liu, Xiangjue Dong, Yanan Li, Deva Ramanan, James Caverlee, and Shu Kong. The neglected tails in vision-language models. In *Proceedings of the IEEE/CVF Conference on Computer Vision and Pattern Recognition (CVPR)*, pp. 12988–12997, June 2024.

Adam Paszke, Sam Gross, Francisco Massa, Adam Lerer, James Bradbury, Gregory Chanan, Trevor Killeen, Zeming Lin, Natalia Gimelshein, Luca Antiga, Alban Desmaison, Andreas Köpf, Edward Yang, Zach DeVito, Martin Raison, Alykhan Tejani, Sasank Chilamkurthy, Benoit Steiner, Lu Fang, Junjie Bai, and Soumith Chintala. Pytorch: An imperative style, high-performance deep learning library, 2019.

Bryan Perozzi, Bahare Fatemi, Dustin Zelle, Anton Tsitsulin, Mehran Kazemi, Rami Al-Rfou, and Jonathan Halcrow. Let your graph do the talking: Encoding structured data for llms. *arXiv preprint arXiv:2402.05862*, 2024.

Yijian Qin, Xin Wang, Ziwei Zhang, and Wenwu Zhu. Disentangled representation learning with large language models for text-attributed graphs. *arXiv preprint arXiv:2310.18152*, 2023.

Rafael Rafailov, Archit Sharma, Eric Mitchell, Christopher D Manning, Stefano Ermon, and Chelsea Finn. Direct preference optimization: Your language model is secretly a reward model. *Advances in Neural Information Processing Systems*, 36, 2024.

Ladislav Rampášek, Michael Galkin, Vijay Prakash Dwivedi, Anh Tuan Luu, Guy Wolf, and Dominique Beaini. Recipe for a general, powerful, scalable graph transformer. *Advances in Neural Information Processing Systems*, 35:14501–14515, 2022.

Nils Reimers and Iryna Gurevych. Sentence-bert: Sentence embeddings using siamese bert-networks. *arXiv preprint arXiv:1908.10084*, 2019.

Xubin Ren, Jiabin Tang, Dawei Yin, Nitesh Chawla, and Chao Huang. A survey of large language models for graphs. *arXiv preprint arXiv:2405.08011*, 2024.

T Konstantin Rusch, Michael M Bronstein, and Siddhartha Mishra. A survey on oversmoothing in graph neural networks. *arXiv preprint arXiv:2303.10993*, 2023.

Pranab Sahoo, Ayush Kumar Singh, Sriparna Saha, Vinija Jain, Samrat Mondal, and Aman Chadha. A systematic survey of prompt engineering in large language models: Techniques and applications. *arXiv preprint arXiv:2402.07927*, 2024a.

Pranab Sahoo, Ayush Kumar Singh, Sriparna Saha, Vinija Jain, Samrat Mondal, and Aman Chadha. A systematic survey of prompt engineering in large language models: Techniques and applications, 2024b. URL `https://arxiv.org/abs/2402.07927`.

Clayton Sanford, Bahare Fatemi, Ethan Hall, Anton Tsitsulin, Mehran Kazemi, Jonathan Halcrow, Bryan Perozzi, and Vahab Mirrokni. Understanding transformer reasoning capabilities via graph algorithms. *arXiv preprint arXiv:2405.18512*, 2024.

V Sanh. Distilbert, a distilled version of bert: Smaller, faster, cheaper and lighter. *arXiv preprint arXiv:1910.01108*, 2019.

Prithviraj Sen, Galileo Namata, Mustafa Bilgic, Lise Getoor, Brian Galligher, and Tina Eliassi-Rad. Collective classification in network data. *AI magazine*, 29(3):93–93, 2008.

Avanti Shrikumar, Peyton Greenside, Anna Shcherbina, and Anshul Kundaje. Not just a black box: Learning important features through propagating activation differences. *arXiv preprint arXiv:1605.01713*, 2016.

Avanti Shrikumar, Peyton Greenside, and Anshul Kundaje. Learning important features through propagating activation differences. In *International conference on machine learning*, pp. 3145–3153. PMLR, 2017.

Karen Simonyan, Andrea Vedaldi, and Andrew Zisserman. Deep inside convolutional networks: Visualising image classification models and saliency maps. *arXiv preprint arXiv:1312.6034*, 2013.

Kaya Stechly, Karthik Valmeekam, and Subbarao Kambhampati. Chain of thoughtlessness: An analysis of cot in planning. *arXiv preprint arXiv:2405.04776*, 2024.

Bing Su, Dazhao Du, Zhao Yang, Yujie Zhou, Jiangmeng Li, Anyi Rao, Hao Sun, Zhiwu Lu, and Ji-Rong Wen. A molecular multimodal foundation model associating molecule graphs with natural language, 2022.

Jiabin Tang, Yuhao Yang, Wei Wei, Lei Shi, Lixin Su, Suqi Cheng, Dawei Yin, and Chao Huang. Graphgpt: Graph instruction tuning for large language models. *arXiv preprint arXiv:2310.13023*, 2023.

Hugo Touvron, Louis Martin, Kevin Stone, Peter Albert, Amjad Almahairi, Yasmine Babaei, Nikolay Bashlykov, Soumya Batra, Prajjwal Bhargava, Shruti Bhosale, et al. Llama 2: Open foundation and fine-tuned chat models. *arXiv preprint arXiv:2307.09288*, 2023.

Keyon Vafa, Justin Y Chen, Jon Kleinberg, Sendhil Mullainathan, and Ashesh Rambachan. Evaluating the world model implicit in a generative model. *arXiv preprint arXiv:2406.03689*, 2024.

Karthik Valmeekam, Matthew Marquez, Sarath Sreedharan, and Subbarao Kambhampati. On the planning abilities of large language models - a critical investigation. In A. Oh, T. Naumann, A. Globerson, K. Saenko, M. Hardt, and S. Levine (eds.), *Advances in Neural Information Processing Systems*, volume 36, pp. 75993–76005. Curran Associates, Inc., 2023. URL `https://proceedings.neurips.cc/paper_files/paper/2023/file/efb2072a358cefb75886a315a6fcf880-Paper-Conference.pdf`.

Ashish Vaswani, Noam Shazeer, Niki Parmar, Jakob Uszkoreit, Llion Jones, Aidan N Gomez, Łukasz Kaiser, and Illia Polosukhin. Attention is all you need. *Advances in neural information processing systems*, 30, 2017.

Petar Veličković, Guillem Cucurull, Arantxa Casanova, Adriana Romero, Pietro Lio, and Yoshua Bengio. Graph attention networks. *arXiv preprint arXiv:1710.10903*, 2017.

Petar Veličković, Guillem Cucurull, Arantxa Casanova, Adriana Romero, Pietro Liò, and Yoshua Bengio. Graph Attention Networks. *International Conference on Learning Representations*, 2018. URL `https://openreview.net/forum?id=rJXMpikCZ`. accepted as poster.

Heng Wang, Shangbin Feng, Tianxing He, Zhaoxuan Tan, Xiaochuang Han, and Yulia Tsvetkov. Can language models solve graph problems in natural language? *Advances in Neural Information Processing Systems*, 36, 2024a.

Jianing Wang, Junda Wu, Yupeng Hou, Yao Liu, Ming Gao, and Julian McAuley. Instructgraph: Boosting large language models via graph-centric instruction tuning and preference alignment. *arXiv preprint arXiv:2402.08785*, 2024b.

Wenhai Wang, Zhe Chen, Xiaokang Chen, Jiannan Wu, Xizhou Zhu, Gang Zeng, Ping Luo, Tong Lu, Jie Zhou, Yu Qiao, et al. Visionllm: Large language model is also an open-ended decoder for vision-centric tasks. *Advances in Neural Information Processing Systems*, 36, 2024c.

Xiao Wang, Houye Ji, Chuan Shi, Bai Wang, Yanfang Ye, Peng Cui, and Philip S Yu. Heterogeneous graph attention network. In *The world wide web conference*, pp. 2022–2032, 2019.

Xuezhi Wang, Jason Wei, Dale Schuurmans, Quoc Le, Ed Chi, Sharan Narang, Aakanksha Chowdhery, and Denny Zhou. Self-consistency improves chain of thought reasoning in language models. *arXiv preprint arXiv:2203.11171*, 2022.

Jason Wei, Xuezhi Wang, Dale Schuurmans, Maarten Bosma, Brian Ichter, Fei Xia, Ed Chi, Quoc Le, and Denny Zhou. Chain-of-thought prompting elicits reasoning in large language models, 2023.

Shengqiong Wu, Hao Fei, Leigang Qu, Wei Ji, and Tat-Seng Chua. Next-gpt: Any-to-any multimodal llm. *arXiv preprint arXiv:2309.05519*, 2023.

Zhanghao Wu, Paras Jain, Matthew Wright, Azalia Mirhoseini, Joseph E Gonzalez, and Ion Stoica. Representing long-range context for graph neural networks with global attention. *Advances in Neural Information Processing Systems*, 34:13266–13279, 2021.

Zhenqin Wu, Bharath Ramsundar, Evan N. Feinberg, Joseph Gomes, Caleb Geniesse, Aneesh S. Pappu, Karl Leswing, and Vijay Pande. Moleculenet: A benchmark for molecular machine learning, 2018.

Zonghan Wu, Shirui Pan, Fengwen Chen, Guodong Long, Chengqi Zhang, and S Yu Philip. A comprehensive survey on graph neural networks. *IEEE transactions on neural networks and learning systems*, 32(1):4–24, 2020.

Keyulu Xu, Weihua Hu, Jure Leskovec, and Stefanie Jegelka. How powerful are graph neural networks? *arXiv preprint arXiv:1810.00826*, 2018.

Shunyu Yao, Dian Yu, Jeffrey Zhao, Izhak Shafran, Tom Griffiths, Yuan Cao, and Karthik Narasimhan. Tree of thoughts: Deliberate problem solving with large language models. *Advances in Neural Information Processing Systems*, 36, 2024.

Junjie Ye, Xuanting Chen, Nuo Xu, Can Zu, Zekai Shao, Shichun Liu, Yuhan Cui, Zeyang Zhou, Chao Gong, Yang Shen, et al. A comprehensive capability analysis of gpt-3 and gpt-3.5 series models. *arXiv preprint arXiv:2303.10420*, 2023a.

Ruosong Ye, Caiqi Zhang, Runhui Wang, Shuyuan Xu, and Yongfeng Zhang. Natural language is all a graph needs. *arXiv preprint arXiv:2308.07134*, 2023b.

Chengxuan Ying, Tianle Cai, Shengjie Luo, Shuxin Zheng, Guolin Ke, Di He, Yanming Shen, and Tie-Yan Liu. Do transformers really perform badly for graph representation? *Advances in neural information processing systems*, 34:28877–28888, 2021.

Zhitao Ying, Dylan Bourgeois, Jiaxuan You, Marinka Zitnik, and Jure Leskovec. Gnnexplainer: Generating explanations for graph neural networks. *Advances in neural information processing systems*, 32, 2019.

Jiaxuan You, Zhitao Ying, and Jure Leskovec. Design space for graph neural networks. *Advances in Neural Information Processing Systems*, 33:17009–17021, 2020.

Hao Yuan, Haiyang Yu, Shurui Gui, and Shuiwang Ji. Explainability in graph neural networks: A taxonomic survey. *IEEE Transactions on Pattern Analysis and Machine Intelligence*, 45(5):5782–5799, 2023.

Seongjun Yun, Minbyul Jeong, Raehyun Kim, Jaewoo Kang, and Hyunwoo J Kim. Graph transformer networks. *Advances in neural information processing systems*, 32, 2019.

Jianan Zhao, Le Zhuo, Yikang Shen, Meng Qu, Kai Liu, Michael Bronstein, Zhaocheng Zhu, and Jian Tang. Graphtext: Graph reasoning in text space. *arXiv preprint arXiv:2310.01089*, 2023.

Yongchao Zhou, Andrei Ioan Muresanu, Ziwen Han, Keiran Paster, Silviu Pitis, Harris Chan, and Jimmy Ba. Large language models are human-level prompt engineers. *arXiv preprint arXiv:2211.01910*, 2022.

A Broader Impacts

Our research aims to enhance the understanding of graph structures through language models (LMs), marking a modest but significant step toward improved graph reasoning capabilities. This foundational effort seeks to refine how LMs interpret complex graph data, aspiring to inspire further research in this domain. Given the exploratory nature of our work, we have not identified specific negative societal impacts or potential for malicious use directly attributable to our research. Nevertheless, we recognize that all technological advancements carry inherent risks.

In alignment with responsible research practices, we suggest continuous monitoring of developments in the application of LMs to graph data analysis. As these models evolve to handle more complex tasks, maintaining vigilance becomes crucial to preemptively address any emerging risks before they manifest. Our commitment to ethical conduct underpins our research methodology, which is designed to avoid harm and does not involve human subjects, thus mitigating potential ethical concerns related to privacy and fairness. By promoting ongoing assessment and adopting a proactive approach to research governance, we aim to ensure that our contributions positively impact the field and adhere to the highest standards of ethical research.

B Further Related Works

Graph Neural Networks (GNNs). Graph Neural Networks (GNNs) have emerged as a powerful framework for learning over graph-structured data (Kipf & Welling, 2017; Gilmer et al., 2017; Veličković et al., 2018; Wu et al., 2020; Liu et al., 2020). GNNs operate by iteratively aggregating information from a node's neighbors, thereby learning node representations that capture the local structure and features of the graph. This message-passing mechanism enables GNNs to be highly effective in tasks such as node classification, link prediction, and graph classification. However, despite their success, GNNs are often challenged by issues such as over-smoothing in deeper networks (Rusch et al., 2023) and difficulties in handling long-range dependencies (Sanford et al., 2024), which can limit their effectiveness on larger and more complex graphs.

Graph Transformer (GT). Graph Transformers (GTs) (Yun et al., 2019; Rampášek et al., 2022) represent a more recent approach that aims to capture global dependencies within graph data using self-attention mechanisms. Inspired by the success of transformers in NLP tasks, GTs adapt the self-attention mechanism to graph-structured data, allowing them to capture both local and global interactions simultaneously. This approach helps address some of the limitations of GNNs in learning long-range dependencies. However, Graph Transformers often require additional architectural complexities (Black et al., 2024), such as centrality encoding, edge features, and spatial encodings, to effectively represent graph structures. These added complexities can lead to increased computational demands and make them less interpretable compared to conventional GNNs.

Transformer Block in Language Models. In a transformer model, each block processes an input sequence $H_i = \{h_1, h_2, \ldots, h_{n_i}\}$ to output an updated sequence H_{i+1}. A transformer block is structured around an attention mechanism and a feedforward network, both supplemented by residual connections and layer normalization. The multi-head attention mechanism processes the sequence H_i, formulated as $\text{Attention}(Q, K, V) = \text{softmax}\left(\frac{QK^T}{\sqrt{d_k}}\right)V$ where Q, K, V are queries, keys, and values derived from H_i, and d_k is the dimension of keys. This output is then combined with the original input H_i and normalized: $\text{Output}_{\text{attention}} = \text{LayerNorm}(H_i + \text{Attention}(H_i))$. Following this, a position-wise feedforward network processes each position in $\text{Output}_{\text{attention}}$, described by $\text{FFN}(x) = \max(0, xW_1 + b_1)W_2 + b_2$ with W_1, W_2, b_1, b_2 as the network parameters. The final output H_{i+1} for the block is computed by applying another layer normalization on the summation of the feedforward network output and the attention output: $H_{i+1} = \text{LayerNorm}(\text{Output}_{\text{attention}} + \text{FFN}(\text{Output}_{\text{attention}}))$. This architecture allows the transformer to capture and process dependencies across the input sequence, enabling deep contextual understanding that propagates through successive layers of the model.

Comparisons to Prior Work. LLM-only methods commonly fail to effectively learn from graph data due to computational feasibility and the loss of graph structural information. In contrast, our model addresses these challenges with a local-to-global hierarchical design that efficiently leverages graph structure. Hybrid

GNN-LM approaches typically encounter problems with task-specific designs and limited interpretability. In comparison, our method is inherently task-agnostic and demonstrates high interpretability. When compared to closely related conventional Graph Transformers, which necessitate complex designs for centrality, edge, and spatial encoding, our method streamlines the process by exclusively using natural language input, eliminating the need for these elaborate encodings.

C Experiment Details

C.1 Details about the Datasets

In this section, we describe in detail the datasets used for our experiments. We first describe the Graph Reasoning dataset followed by the real world datasets.

C.1.1 Graph Reasoning

Several works have proposed benchmarks for graph reasoning, such as the NLGraph (Wang et al., 2024a) and GraphQA (Fatemi et al., 2023). However, upon closer examination, we observed that these benchmarks suffer from significant class imbalance, with some classes having far more data points than others. For example, in the cycle dataset of GraphQA, 82% of the data samples contain at least one cycle. Some works like Graphtoken (Perozzi et al., 2024) have leveraged this dataset, with their proposed architecture achieving 83% accuracy on the cycle dataset. This raises concerns about whether the models are truly reasoning on the datasets or simply making majority label predictions. Additionally, the majority of graphs in these benchmarks have a small number of nodes, typically ranging from 5 to 20. In reality, we expect real-world graph datasets to be much larger than this.

To address these issues, we propose a new benchmark constructed using a random graph generator. Importantly, all datasets in our benchmark are balanced, enabling us to evaluate the true graph reasoning ability of language models accurately. Training and validation graphs contain up to 40 nodes with test set containing exactly 40 nodes. .

In this section we describe our random graph generator used for creating graph reasoning datasets.

Pre-defined graphs To ensure that our generator is well covered, we first include common graphs including Cyclic graphs, Star graphs, Complete graphs, Path graphs, Tree graphs, Wheel graphs and Barbell graphs. All of these graphs can be created using NetworkX documentation[1].

Random graphs A graphon is a function $W : [0,1]^2 \rightarrow [0,1]$ that takes 2 values v_1, $v_2 \in [0,1]$ for each pair of nodes and returns the probability $p \in [0,1]$ for an edge between these 2 nodes. The function W can be any function that takes 2 values v_1, $v_2 \in [0,1]$ and returns $p \in [0,1]$. Given two values v_1 and v_2, we implement following functions:

1. Constant graphon: Returns a random number $p \in [0.3, 0.7]$
2. Sparse graphon: Returns a small random number $p \in [0.05, 0.15]$
3. Dense graphon: Returns a big random number $p \in [0.8, 1.0]$
4. Linear graphon: Returns $p = v_1 * v_2$
5. Quadratic graphon: Returns $p = v_1^2 * v_2^2$
6. Sigmoidal graphon: Returns $p = \frac{1}{1+\exp(-10(u-v))}$
7. Step graphon: Returns $p = 1$ if $v_1 \geq t$ and $v_2 \geq t$ for some random threshold $t \in [0,1]$

[1] https://networkx.org/documentation/stable/index.html

8. Sin graphon: Returns $p = \sin(\pi v_1) \cdot \sin(\pi v_2)$
9. Avg graphon: Returns $p = (v_1 + v_2)/2$
10. Exp. decay graphon: Returns $p = \exp(-(v_1^2 + v_2^2))$
11. Softmax graphon: Returns $p = \frac{\exp(v_1)}{\exp(v_1)+\exp(v_2)}$

The value v_i for the ith node is randomly initialized for each node. Using these formulations, we prepare our benchmark for structural reasoning tasks. For every task, we extract a graph from our Random Graph Generator and assign it a label depending on the task. We collect equal number of graphs for every label to prevent bias towards majority class.

Table 6: Summary of Graph Analysis Tasks and Their Dataset Specifications

	Distance	**Cycle Detection**	**Edge Count**	**Reachability**	**Edge Existence**	**Connected Components**	**Node Degree**
#Classes	6	2	70	2	2	38	39
Dataset Size Used	20000	4000	14000	4000	4000	19000	8000

Armed with the general-purpose graph dataset generator, we adapt synthetically generated graphs to various graph reasoning tasks with varying complexities and describe the problem setups in a structured manner. Specifically, we first generate subsets of base graphs for each task by controlling node quantity and graph density. We then tailor these base graphs for specific tasks and design queries to assess the models' capabilities accordingly. These 7 datasets summarized in Table 6 are detailed below. A random split of 80/10/10 is used for training , validation and test sets.

- **Task 1: Shortest Distance**
  Given a graph $G = \{V, E\}$, predict the shortest distance between two nodes v_i and v_j, categorized into six classes from 0 to 5. Class 0 indicates no path exists, while classes 1 to 5 represent distances from 1 to 5 edges. The query posed is: "What is the shortest distance between nodes 0 and 1?"

- **Task 2: Cycle Detection**
  In a graph $G = \{V, E\}$, determine if a cycle exists. The task classifies graphs into two categories: presence or absence of a cycle. The question asked is: "Is the graph cyclic?"

- **Task 3: Edge Count**
  Our random graph generator can produce graphs with over 700 edges. To minimize the required training size, we categorize sets of 10 edges into a single class. Specifically, graphs with 1 to 10 edges are classified as class 0, 11 to 20 as class 1, continuing in this manner up to 691 to 700, which are classified as class 69. The query posed is: "What is the total number of edges in the graph?"

- **Task 4: Reachable**
  In a graph $G = \{V, E\}$, predict whether there is a reachable path between two nodes v_i and v_j. The query for this task is: "Are nodes 0 and 1 reachable from each other?"

- **Task 5: Edge Existence**
  Determine if an edge exists between two nodes in a graph, represented as $G = \{V, E\}$. The posed query is: "Does an edge exist between nodes 0 and 1?"

- **Task 6: Connected Components**
  Predict the number of connected components in a graph $G = \{V, E\}$. A component is a set of nodes that are reachable from one another. Specifically if $v_i \in C_1$ and $v_j \in C_2$ where C_1 and C_2 are different components then there exists no path from v_1 to v_2. The query is: "How many connected components does the graph have?"

- **Task 7: Node Degree**
  Estimate the degree of a node in the graph, representing the number of direct connections or neighbors the node has. The question is: "What is the degree of node 0?"

C.1.2 Real world datasets

We conduct experiments on 7 different Text Attributed Graph (TAG) datasets. All of these graphs have node features available in natural language. The datasets are concisely summarized in the table below, followed by detailed descriptions of each dataset.

Table 7: Datasets summary for real world graphs with text attributes

Dataset	Domain	Task	# Graphs	Avg. #Nodes	Avg. #Edges	# Classes
Cora	Citation	Node	1	2,708	10,556	7
ogbn-arxiv	Citation	Node	1	169,343	1,166,243	40
PubMed	Citation	Node	1	19,717	44,338	3
PubMed	Citation	Link	1	19,717	44,338	2
FB15k-237	Knowledge	Link	1	14,541	310,116	237
WN18RR	Knowledge	Link	1	40,943	93,003	11
HIV	Molecule	Graph	41,127	25.5	27.5	2

Cora dataset, sourced from the GitHub repository as described in Chen et al. (2024c) , is a citation network in the computer science domain. Each node in this dataset represents a research paper, with raw text features consisting of the paper's title and abstract. The edges between nodes indicate citation relationships. Nodes are labeled according to the category of the paper, encompassing seven possible classes. For our study, we focus on node-level prediction, specifically predicting the category of each paper based on its features and structure. We use the 60-20-20 random split for training, validation and testing.

PubMed dataset comprises 19,717 scientific publications from the PubMed database, specifically related to diabetes, categorized into one of three classes. The citation network includes 44,338 links. Each node represents a research paper, with raw text features including the paper's title and abstract. Our study involves both node classification and link classification tasks on the PubMed dataset. The raw text data of PubMed dataset was collected from GitHub repository provided in Chen et al. (2024c).

For node classification, we use a 60-20-20 random split for training, validation, and testing. For link classification, the goal is to predict whether two nodes are directly connected. Following the methodology of OFA (Liu et al., 2024a), we use an 85-5-10 random split. In the link classification task, The training, validation and testing set is created using existence edges as positive samples and an equal number of negative samples by checking for the absence of an edge between nodes. The evaluation metric for the link-level task is the AUC.

ogbn-arXiv[2] is a directed graph representing the citation network among Computer Science (CS) arXiv papers. The task involves predicting the 40 subject areas of these papers, such as cs.AI, cs.LG, and cs.OS, which are manually labeled by the authors and arXiv moderators. We follow the standard split for this dataset: training on papers published until 2017, validating on those from 2018, and testing on papers published since 2019. The raw text data of the ogbn-arxiv was collected using the same protocol as the GitHub repository provided in Prodigy (Huang et al., 2024).

Molhiv[3] dataset is a molecular property prediction dataset adopted from the MoleculeNet (Wu et al., 2018). The dataset contains 41127 molecules each represented as a graph with atom as nodes and bonds as edges. Each atom has 9 discrete features. 1 of the features (Chirality) is common for all atoms and is therefore not considered. The rest of the features are: Atomic Number, Degree of atom, Formal charge, Number of connected Hydrogen, Radical electrons, Hybridization, Aromaticity and Ring. These features can be converted to natural language using only a few lines of code. Similarly the bonds between any 2 atoms can be of 4 types: single, double, triple or aromatic. Each of these bonds also has a boolean property: conjugated. Therefore any edge can be represented using the bond type and whether or not it is conjugated.

[2]ogbn-arXiv is released under license ODC-BY.
[3]ogbg-molhiv is released under license MIT.

Here we perform graph level classification where objective is to classify a molecule as HIV inhibitor or not. The metric used here is AUC.

WN18RR is a link prediction dataset created from WN18, which is a subset of WordNet. WN18RR dataset contains 93,003 triples with 40,943 entities and 11 relation types. Here we perform link classification where we classify any edge in 11 possible edge types. This dataset is extracted from GitHub repository[4].

FB15k-237 is a knowledge graph that contains knowledge base relation triples and textual mentions of Freebase entity pairs. It contains 310,116 triples with 14,541 entities and 237 relation types. Here we perform link classification where we classify any edge in 237 possible edge types. The raw text data of nodes in FB15K237 was collected from the same Github repository as WN18RR.

C.2 Training and Optimization Settings

For the graph reasoning datasets, we train our model from scratch, with the input being the natural language description of the graph structure. In the local block, we employ a BERT-like architecture utilizing a special intra-node masking scheme that masks out language tokens belonging to different nodes. Across all reasoning datasets, we use 4 local block layers. For the global block, we utilize 2 layers for most datasets, except for the Shortest Distance, Edge Count and Number of Connected Components datasets, where 3 global block layers are used. Our observations indicate that more complex tasks benefit from an increased number of global block layers, which enhances overall performance.

We adopt the Adam optimizer (Kingma & Ba, 2014) throughout the training phase, with a learning rate of $5e^{-6}$, weight decay of 0.1, $\beta_1 = 0.9$, and $\beta_2 = 0.95$. Across all datasets, the training consists of 5 epochs, with a batch size of 16 for graph reasoning datasets and 8 for real-world datasets. The shared parameters for all tasks and datasets used in our language model $M_L(G)$ are summarized in Table 8.

Table 8: Parameters used for the language model.

Parameter	**Value**
Activation	gelu
Attention Dropout	0.1
Dimension	768
Dropout	0.1
Hidden Dimension	3072
Max Position Embeddings	4096
Number of Heads	12
Number of Local Block Layers	6

We attempted to leverage pretrained models such as BERT (Devlin et al., 2018), SBERT (Reimers & Gurevych, 2019), DistilBERT (Sanh, 2019), and Llama 2 7B (Touvron et al., 2023) as the lower block, but found no performance gains on graph reasoning tasks; in fact, performance declined when these models were not fine-tuned. This suggests that these pretrained models do not acquire graph structure-related information during pretraining. Our experiments indicate that fine-tuning just 4 layers of the lower block is sufficient to achieve state-of-the-art performance on graph reasoning tasks.

For real-world datasets (Tables 3, 4, and 5), we employ DistilBERT in the local block and fine-tune it. Given that these datasets contain textual node and edge features, pretrained models are better equipped to understand these features. The number of higher block layers for each dataset is set as follows: 4 for Cora, Pubmed, WN18RR, and FB15k-237, 2 for molhiv, and 6 for Arxiv.

[4] https://github.com/villmow/datasets_knowledge_embedding/tree/master

Table 9: Performance comparison with different text encoders for Cora and Pubmed.

	DistilBERT	**SBERT**	**Llama-2**
Cora	87.9%	88.9%	**89.2%**
Pubmed	94.1%	93.9%	**94.9%**

We observed that using larger models yields improved performance on node-level tasks, as depicted in Table 9. This is expected since node features play a more critical role in making accurate node-level predictions within real-world datasets and these larger models are better equiped to understand these text based features.

C.3 Software and Hardware

Our implementation is under the architecture of PyTorch (Paszke et al., 2019) and PyG (Fey & Lenssen, 2019). The deployment environments are Ubuntu 18.04 with 48 Intel(R) Xeon(R) Silver 4214R CPU @ 2.40GHz, 755GB Memory, and graphics cards NVIDIA RTX A6000.

D Additional Experiment Results

D.1 Downstream Task Performance

To assess the adaptability and transferability of our proposed model across different graph domains and task levels, we evaluated its performance on downstream tasks. Specifically, we examined how well the model, when trained on one task level (e.g., node, link, or graph), could adapt to perform effectively on another.

Experimental Setup: We pretrained our model on three distinct datasets representing different task levels: Arxiv (Node-level), Molhiv (Graph-level), and Pubmed (Link-level). Each pretrained model was then fine-tuned on a variety of downstream tasks by updating only the final classification layer for 5 epochs with a learning rate of $4e^{-5}$. This setup allowed us to evaluate the model's ability to leverage learned knowledge and adapt to completely different downstream tasks.

Results and Analysis: The results in Table 10 demonstrate the impressive transferability of our model. For example, the model pretrained on the Arxiv (Node-level) dataset achieved an 87.8% accuracy on the PubMed Link task, outperforming the performance of fully trained GIN despite being trained exclusively on node-level information initially. Similarly, the model pretrained on the Molhiv (Graph-level) dataset delivered competitive results on both node-level (Cora) and link-level (PubMed) tasks, showcasing its ability to adapt to diverse task requirements.

These insights highlight the versatility of our approach, indicating that our model can effectively generalize knowledge from one graph domain to another. Our language model design not only captures graph structures efficiently but can also be fine-tuned for a wide range of downstream applications with limited training, making it a valuable asset for practical real-world applications.

Table 10: Downstream task performance with different pretraining datasets. The model's performance was evaluated after fine-tuning only the classification layer for 5 epochs.

Pretrained \Downstream	**Cora (Node)**	**Pubmed (Node)**	**Pubmed (Link)**	**Molhiv (Graph)**
Arxiv (Node)	80.6	83.8	**87.8**	72.2
molhiv (Graph)	73.9	75.4	86.6	-
Pubmed (Link)	71.6	77.5	-	72.5

D.2 Generation tasks

The current architecture employs local and global transformer blocks and a classification layer for final prediction. For generation on graphs, we need a Decoder model that can generate the output. For this, we take inspiration from GraphLLM (Chai et al., 2023) and leverage Prefix-Tuning (Li & Liang, 2021) for fine-tuning a Frozen Decoder LLM with HLM-G encoder.

Prefix Tuning Given a pre-trained LLM with an L-layer transformer, prefix tuning prepends K trainable continuous tokens (prefixes) to the keys and values of the attention at every transformer layer. Taking the l-th attention layer as an example ($l < L$), prefix vectors $\boldsymbol{P}_l \in \mathbb{R}^{K \times d^{\mathrm{M}}}$ is concatenated with the original keys $\boldsymbol{K}_l \in \mathbb{R}^{* \times d^{\mathrm{M}}}$ and values $\boldsymbol{V}_l \in \mathbb{R}^{* \times d^{\mathrm{M}}}$, where d^{M} is the dimension of LLM, formulated as:

$$\boldsymbol{K}_l' = [\boldsymbol{P}_l; \boldsymbol{K}_l]\,;\ \boldsymbol{V}_l' = [\boldsymbol{P}_l; \boldsymbol{V}_l] \in \mathbb{R}^{(K+*) \times d^{\mathrm{M}}}$$

The new prefixed keys $\boldsymbol{K}_l'$ and values $\boldsymbol{V}_l'$ are then subjected to the l-th attention layer of LLM. For simplicity, we denote the vanilla attention computation as $\boldsymbol{O}_l = \texttt{Attn}(\boldsymbol{Q}_l, \boldsymbol{K}_l, \boldsymbol{V}_l)$. The computation of attention becomes:

$$\boldsymbol{O}_l = \texttt{Attn}(\boldsymbol{Q}_l, [\boldsymbol{P}_l; \boldsymbol{K}_l], [\boldsymbol{P}_l; \boldsymbol{V}_l])$$

We introduce three distinct datasets tailored for graph generation tasks, each with unique complexities and requirements. These tasks are designed to evaluate the model's ability to generate graph structures and properties accurately.

- **Task 1: Shortest Path**
  The objective of this task is to generate the shortest path between two specified nodes in a graph. Given a graph G, the query Q_G is formulated as: "What is the shortest path from node i to j?", where i and j are valid nodes within G. The output is considered correct only if the path generated is both valid and the shortest possible.
- **Task 2: Bipartite Detection**
  This task aims to determine whether a given graph is bipartite. A graph is defined as bipartite if it contains no odd cycles. The challenge for the model is to predict if the graph is bipartite or, if not, to generate an odd cycle. The query Q_G is: "Is the graph bipartite?". An output is deemed correct if it accurately predicts whether the graph is bipartite or identifies an odd cycle when the graph is not bipartite.
- **Task 3: Edge Count**
  This dataset involves predicting the exact number of edges in a graph, enhancing the edge count task detailed in Section 4. Unlike the previous version, this task does not classify edges into pooled groups but requires an exact count. Additionally, the training set does not include all edge counts present in the test set, introducing unseen scenarios. The query Q_G is: "What are the number of edges in the graph?". Correctness is strictly judged on the model's ability to match the exact number of edges in G.

Table 11: Performance comparison for zero shot and HLM-G encoder on different generation tasks. Llama-2 7B is used as a decoder in both settings. (across 1 random run).

	Shortest Path	Bipartite Detection	Edge Count
Zero shot	5.2%	11.7%	2.1%
HLM-G encoder	93.4%	95.1%	92.5%

This data indicates that HLM-G has substantial potential as a powerful graph encoder. The high accuracy across different tasks in our tests demonstrates its effectiveness. Further experiments are necessary to fully explore the zero-shot and few-shot capabilities of HLM-G. These future studies will help validate the model's performance across a broader range of graph-based applications, potentially establishing HLM-G as a useful tool in for leveraging LLMs on graphs.

D.3 Computational Efficiency

We systematically compare the training efficiency across various LLM-based methods on graph reasoning datasets and real world dataset.

Graph Reasoning Datasets. Our study evaluates multiple fine-tuning approaches, which we categorize into two primary groups: Hybrid GNN-LLM fine-tuning and LLM-only fine-tuning. We present training times for GraphToken (a hybrid method), BERT, Llama 3 (LLM-only), and our proposed HLM-G model (LLM-only fine-tuning). GraphToken utilizes a 4-layer GCN as its GNN encoder with approximately 5.2 million training parameters, resulting in a total parameter count of around 8 billion, comparable to the Lora-trained Llama 3. For BERT, we adopt a 4-layer architecture with four attention heads, yielding 56 million parameters. The parameter count for our HLM-G model varies depending on the dataset, comprising 82 million parameters for tasks such as distance, edge count, and the number of components, and 77 million for reachability, cycle, and edge existence datasets.

Table 12 offers a comprehensive comparison of training times among various fine-tuning methods. Despite the HLM-G model having 20 to 30 million more parameters than BERT, its hierarchical dual-block architecture significantly reduces both the training time per epoch and the total time to convergence. In contrast, GraphToken, while achieving shorter training times per epoch, requires a substantially higher number of epochs to reach convergence due to its use of a GCN encoder. Additionally, the training times for Llama 3 are notably high, as expected, due to the model's extensive number of parameters and the maximum input prompt length of 4096, which necessitates longer training durations. In comparison, our HLM-G model exhibits considerable improvements in training efficiency, highlighting the computational advantages of our approach, especially in managing large-scale graph reasoning tasks.

Table 12: **Training time and total training time comparison across graph reasoning datasets.** The total training time refers to the duration required to reach the optimal validation checkpoint.

Dataset	**GraphToken**		**Llama 3**		**BERT**		**HLM-G (ours)**	
	Time/Epoch	Total Time	Time/Epoch	Total Time	Time/Epoch	Total Time	Time/Epoch	Total Time
Distance	30 mins	20 hours	17 hours	34 hours	2 hours 30 mins	7.5 hours	2 hours	6 hours
Reachability	9 mins	8 hours	6 hours	30 hours	2 hours	10 hours	45 mins	1 hour 30 mins
Cycle	9 mins	12 hours	7 hours	21 hours	45 mins	1 hour 30 mins	40 mins	40 mins
Edge Count	33 mins	36 hours	12 hours	48 hours	3 hours 30 mins	24.5 hours	3 hours	6 hours
Edge Existence	9 mins	8.5 hours	6 hours	24 hours	45 mins	1 hour 30 mins	40 mins	40 mins
Connected Components	15 mins	18 hours	12 hours	36 hours	2 hours	14 hours	1 hour	12 hours
Node Degree	17 mins	12 hours	11 hours	33 hours	1 hour 30 mins	6 hours	1 hour	1 hour

Real-world Datasets. We evaluated the training times of our model, HLM-G, against InstructGLM for node and link prediction tasks, as InstructGLM does not support graph-level tasks. For graph-level tasks, we compared HLM-G with Mamba. InstructGLM uses Llama-2 7B as its backbone and incorporates Lora with a rank of 16, resulting in 8.2 million trainable parameters. The trainable parameter count for Mamba is approximately 91.8 million. For HLM-G, the number of trainable parameters varies depending on the number of layers in the higher block (as detailed in Appendix C.2), ranging from 76 million for Molhiv to 86 million for datasets such as Pubmed, Cora, and knowledge graphs, and up to 96 million for Arxiv.

Table 13: **Training time and total training time comparison across real-world datasets.** Total training time refers to the duration required to reach the optimal validation checkpoint.

Dataset	**Mamba**		**InstructGLM**		**HLM-G (ours)**	
	Time/Epoch	Total Time	Time/Epoch	Total Time	Time/Epoch	Total Time
Pubmed Node	-	-	23 hours 10 mins	69 hours 30 mins	2 hours 5 mins	2 hours 5 mins
Pubmed Link	-	-	23 hours 10 mins	46 hours 20 mins	10 hours 30 mins	21 hours
Arxiv	-	-	105 hours	210 hours	7 hours	28 hours
WN18RR	-	-	34 hours	68 hours	2 hours 10 mins	4 hours 20 mins
FB15k-237	-	-	56 hours	56 hours	5 hours	25 hours
Molhiv	6 hours	150 hours	-	-	3 hours	18 hours

Table 13 presents a comparison of training times across real-world datasets, demonstrating the computational efficiency of our HLM-G model relative to other fine-tuned language models. The results clearly highlight HLM-G's capability to perform graph-based tasks efficiently while maintaining high performance. Particularly notable is the significant reduction in training time compared to InstructGLM, especially in larger datasets. This efficiency underscores where our model is most useful.

The real-world datasets used in these comparisons are characterized by their immense size and complex descriptions, factors that typically challenge traditional LLMs. Our HLM-G model is specifically designed to excel in these environments. Unlike conventional LLMs, which may struggle with the scale and specificity of graph-based data, HLM-G leverages its hierarchical architecture to process such data more effectively. This design enables HLM-G to handle the intricate details and vast data volumes more adeptly, making it particularly suited for tasks involving extensive real-world graphs. This advantage makes HLM-G a preferred tool for applications requiring robust and efficient graph reasoning capabilities.

E Interpretation

E.1 Interpretation Ground Truth

In the context of graph reasoning datasets, any graph can be partitioned into two distinct sets of nodes: *citical ground truth nodes*, which are directly responsible for the final prediction, and *non-critical nodes*, which do not influence the prediction either directly or indirectly. Due to the importance of focusing on structurally relevant nodes, we exclude datasets such as components and edge count where each node is integral to the final prediction. This exclusion is crucial as it allows us to experimentally investigate our model's attention mechanisms towards nodes that are truly significant in the reasoning process. Detailed ground truth sets for 3 link-level and 1 node-level task are described below.

Edge Existence In the edge existence task between two nodes u and v, the nodes u and v themselves are sufficient for determining the presence of an edge, thus forming the ground truth:

$$GT = \{u, v\}$$

Shortest Distance For the shortest distance between nodes u and v, ground truth nodes include all nodes lying on any shortest path. Let l be the shortest path length, then ground truth is simply union over all these nodes:

$$GT = \bigcup_{i=1}^{m_l} \{u, a_1^i, a_2^i, \ldots, a_{l-1}^i, v\}$$

where m_l is the number of shortest paths.

Reachability Dataset Unlike the shortest path dataset, reachability requires consideration of all nodes in all possible paths from u to v, including those beyond the shortest path. If n is the total number of nodes in the graph, the ground truth set includes:

$$GT = \bigcup_{j=l}^{n-1} \bigcup_{i=1}^{m_j} \{u, a_1^i, a_2^i, \ldots, a_{j-1}^i, v\}$$

where m_l is the number of paths of length j, $j \in \{l, l+1...n-1\}$. This represents a more holistic understanding of the graph's connectivity by including paths of length l through $n-1$.

Node Degree For node degree tasks focused on a single node u, the determination of degree relies solely on its direct connections to other nodes in the graph.. The ground truth is straightforward in this case:

$$GT = \{u\}$$

Together, these definitions facilitate a comprehensive evaluation of our model's capability to handle various structural reasoning tasks, each necessitating a specific set of nodes as ground truth based on task requirements.

E.2 Explanation as Interpretation

It is challenging to compare interpretability performance with methods that are not interpretable or have different interpretation formats. To achieve such comparisons, we propose to use explanations of models as interpretations. [5] However, explanations provided by explainers face their possible performance issue that the produced explanations might not be faithful to the deep model behaviors.

This faithfulness issue requires us to first discover the most faithful explanations for the models before using them as model interpretations. Therefore, instead of using one explainer, we adopt four explainers to select the best explanation for each model on each dataset including Saliency (Simonyan et al., 2013), Input $\times$ Gradient (Shrikumar et al., 2016), DeepLIFT (Shrikumar et al., 2017), and GNNExplainer (Ying et al., 2019), where GNNExplainer can be only applied to GNNs. Specifically, we adopt Fidelity- (Yuan et al., 2023), a.k.a., sufficiency Fidelity (Gui et al., 2023), to measure whether an explanation provided by an explainer is faithful to the model behavior. Formally, given N samples, Fidelity can be written as

$$\text{Fidelity} = \frac{1}{N}\sum_{i=1}^{N}\left(\mathbb{1}(\hat{y}_i = y_i) - \mathbb{1}(\hat{y}_i^{\boldsymbol{r}_i^k} = y_i)\right), \tag{1}$$

where the sample index i is used as subscription; $\mathbb{1}(\cdot) = 1$ when the given condition is satisfied, otherwise, 0; $\hat{y}_i^{\boldsymbol{r}_i^k}$ indicates the sample i's prediction result using only the top-k important nodes.

Since high Fidelity indicates that the explanation directly reflects the model behavior, the explanation can be used as the model behavior representative. In the experiment, for each dataset and each method, we select the explanation with the highest average Fidelity from all explainers. The Fidelity results are plotted in Figure. 4, where Sparsity denotes the ratio $1 - k/n$; thus, higher Sparsity indicates less important nodes are used.

It is crucial to note that Fidelity results do not reflect the interpretability performance of models, they only show the relation between the explainer and the model and are used as a principle to choose the right explainer for each model on each dataset. With the best explanation, we use it as the interpretation of the model to conduct interpretability comparisons mentioned in Section 4.2.2.

E.3 Interpretation Visualization

We present the interpretation results in Figures 5 and 6. As depicted, important tokens are highlighted with a green background. The methods under comparison are required to count the nodes connected to node 0 for making predictions. While our method accurately processes this task, BERT fails to correctly identify the relevant node for degree counting. This discrepancy arises because node 0, consistently presented at the beginning during training, is permuted during testing, causing BERT to misidentify its position. In contrast, our method employs a permutation-invariant approach to graph processing, thereby preserving its high performance during testing.

E.4 Local Block Analysis

The assessment of the node structure annotation embeddings in HLM-G reveals intriguing insights into the model's encoding capabilities. These embeddings, derived from 1-hop neighborhood information, prompt an inquiry into the model's approach to capturing such local graph structures. Specifically, we investigate the positional and structural awareness exhibited by these embeddings, akin to the strategies employed in GNNs and GTs, where Positional Encoding (PE) (Dwivedi et al., 2022) is a common technique for enhancing model performance. PE assigns similar positional values to nodes in close proximity, reflecting their relative positions within the graph.

To evaluate the positional and structural encoding prowess of HLM-G, we create over 10000 pairs of nodes and analyze the node structure annotation embeddings generated by the lower layers of the model. By

[5] Note that explainers provide post explanations that can be applied to any models, while interpretations are generally produced by the model's specific design, a.k.a., self-interpretable model.

comparing these embeddings using cosine similarity, we categorize the pairs into three groups based on their hop distance: 1-hop neighbors, 2-hop neighbors, and neighbors at 3 or more hops.

Table 14: **Cosine similarity of 1-hop and 2-hop neighbors with different numbers of common neighbors.** We see that cosine similarity between 1-hop and 2-hop neighbours is quite high and keeps on increasing with increasing number of common neighbors.

Common Neighbors	1-hop Neighbors	2-hop Neighbors
1	0.956	0.931
3	0.957	0.939
5	0.966	0.954
7	0.972	0.951
9	0.975	0.968

Table 15: **Similarity for 3-hop neighbors (no common neighbors) based on the difference of structure.** The table suggests that lower block assigns similar embedding to nodes that share a common 1-hop structure.

Difference of Node Degree	Cosine Similarity
0	0.955
1	0.839
2	0.557
3	0.024
4	-0.113
5	-0.129
6	-0.135

Table 14 and Table 15 reveals a consistent trend in similarity: embeddings of 1-hop neighbors exhibit higher similarity compared to those of 2-hop neighbors, and likewise for 3+ hop neighbors. Furthermore, we observe that the number of common neighbors between two nodes significantly influences the similarity of their embeddings. A higher number of common neighbors indicates greater positional similarity between the nodes.

In the case of 3+ hop neighbors where no common neighbors exist, we evaluate the role of structural similarity. Here, nodes are considered similar in structure if they share a similar 1-hop neighborhood, specifically in terms of the number of neighbors. The analysis demonstrates that the greater the difference in 1-hop structure between nodes, the lower the similarity in their embeddings. This suggests that HLM-G effectively encodes 1-hop neighborhood information, assigning higher similarity to nodes that are either positionally or structurally similar.

F Ablation Studies

F.1 Pooling Mechanisms

In the process of constructing node embeddings from the outputs $(H_{U^{AE}}, H_{U^X})$ of the lower layer, we examine two distinct pooling mechanisms: mean pooling and concatenate pooling.

Mean pooling employs a parameter α, which signifies the relative importance attributed to structural information. Specifically,

$$\boldsymbol{z}_v = \text{Pool}(H_{U^{AE}}, H_{U^X}) = \alpha * H_{U^{AE}} + (1 - \alpha) * H_{U^X}$$

Essentially, each neuron within $\boldsymbol{z}_v$ encapsulates both structural and feature information. An $\alpha > 0.5$ indicates a predominance of structural information in the final prediction process, whereas $\alpha < 0.5$ suggests that nodal

features hold greater significance.

Concatenate pooling, in contrast, yields node embeddings of doubled dimensionality by concatenating structural and feature embeddings,

$$\boldsymbol{z}_v = \text{Pool}(H_{U^{AE}}, H_{U^X}) = \text{concat}(H_{U^{AE}}, H_{U^X})$$

This approach integrates structural and feature vectors, thereby expanding the representational capacity of the resultant node embeddings. The impact of various pooling ratios (α) is systematically evaluated across one node-level, link-level and graph-level real-world datasets.

Table 16: **Performance comparison between mean pooling and concatenate pooling** across node- link- and graph- level datasets. $\uparrow \alpha$ implies more structural information is used for making final predictions. Metric is Accuracy for cora and ROC-AUC for molhiv and PubMed. $\alpha = 0$ implies only node features are used for making final prediction whereas $\alpha = 1$ means that predictions rely entirely on the graph's structure.

Pooling		**Cora**	**molhiv**	**PubMed**
	α	Node	Graph	Link
	0.0	86.32	73.8	95.7
	0.1	87.06	74.2	94.8
	0.2	**88.45**	75.5	96.2
Mean	0.3	86.9	**76.39**	97.2
	0.4	86.3	74.2	97.4
	0.5	85.9	74.5	**98.24**
	0.6	85.58	75.6	98.2
	1.0	66.35	75.1	91.1
Concatenate	-	85.35	75.1	96.6

Table 16 shows that mean pooling generally outperforms concatenate pooling, with α values between 0.1 and 0.5 delivering consistently strong results across all datasets. It's crucial to recognize that α measures the structural relevance in the final model. Our findings suggest that features specific to individual nodes are more significant than broader structural characteristics, especially in citation networks such as Cora, where $\alpha = 0.1$ is optimal. Conversely, for the PubMed link dataset, an α value of 0.5 yields the best performance, reflecting the importance of structural connections in conveying critical information about the relationships between nodes.

F.2 Input Prompt Design

Various prompt designs can be employed to describe graph structures for language models. While the main paper predominantly used a natural language description focusing on 1-hop neighbors (our Current Graph Description Language, CGDL), it's important to assess whether different prompt styles impact the model's performance. In this ablation study, we explore two additional prompt styles: the Adjacency List Format (Adj-List) and Edge List Format (Edges).

Moreover, we investigate the model's out-of-domain (OOD) capabilities under two scenarios:

- **Cross-Prompt Evaluation:** In this setting, models trained on one prompt design (e.g., CGDL) are evaluated on different prompt designs (e.g., Adj-List or Edges) to test adaptability.
- **Node Token Variability:** We introduce OOD test sets where node identifiers are replaced with random strings of up to four characters, simulating a situation where node tokens during inference differ from those encountered during training.

Experimental Setup: We conducted our experiments on the Cycle graph reasoning dataset, where we trained separate models using each of the three prompt designs—CGDL, Adj-List, and Edges. Each model

was trained independently using the respective prompt format to ensure it could learn the graph structures as described by that particular design. Following training, these models were evaluated on all three prompt formats, as well as their OOD versions with altered node tokens, resulting in a comprehensive assessment of both in-domain and out-of-domain performance. This setup allowed us to rigorously test the adaptability and robustness of our model under varying prompt styles and node token representations.

Table 17: **In-domain and Out-of-domain performance analysis across different prompt styles and node token variations on cycle dataset.** Performance is measured as accuracy (%).

Training \Testing	CGDL	Adj-List	Edges	CGDL-OOD	Adj-List-OOD	Edges-OOD
CGDL	**99.5%**	52.5%	54.1%	**96.0%**	51.9%	53.6%
Adj-List	93.2%	**98.5%**	74.2%	73.2%	**94.2%**	66.5%
Edges	94.5%	86.0%	**99.0%**	89.5%	78.1%	**98.7%**

Key Observations:

1. **Strong In-Domain Performance:** The diagonal entries in Table 17 (99.5%, 98.5%, and 99.0%) indicate that each model performs exceptionally well when evaluated using the same prompt style as the one it was trained on, demonstrating strong in-domain performance. This suggests that our model is capable of effectively learning graph structures regardless of the chosen prompt style.

2. **Resilience to Node Token Variability:** When examining the OOD results where node tokens were changed (CGDL-OOD, Adj-List-OOD, Edges-OOD), each model retained considerable accuracy compared to its in-domain results. For example, the model trained on the Edges format maintained a high performance of 98.7% in the Edges-OOD setting. This suggests that the model is robust against variations in node tokens and can maintain its graph structure understanding even when faced with different node representations.

3. **Superior Generalization with Edge Descriptions:** The model trained with the Edges format demonstrated remarkable generalization ability across both cross-prompt settings and OOD scenarios. It achieved high accuracy when tested on different prompt designs (e.g., 94.5% on CGDL and 86.0% on Adj-List), and similarly performed well even when node tokens were altered. This indicates that training on the Edges format enables the model to adapt more effectively to variations in graph description languages and node representations, making it a versatile choice for different graph tasks.

Overall, this ablation study on input prompt design reveals that our model can handle different input prompt designs and adapt to node token variations, showcasing its strong generalizability and robustness in capturing graph structures across diverse graph description languages.

F.3 Local Block Design

In this section, we examine different architectural approaches for the local block of our model, focusing on how structure and node features are processed. Traditionally, these features are handled hierarchically, meaning they are processed independently from each other. The input to the hierarchical design lower block is structured as follows:

$$U_G = (\text{concat}(U_1^X, U_1^{AE}), \text{concat}(U_2^X, U_2^{AE}), \ldots, \text{concat}(U_n^X, U_n^{AE}), U_Q)$$

This approach employs a single lower block, M_L, which processes the concatenated features hierarchically.

Following the hierarchical model, we introduce a double hierarchical design, which further divides the handling of node and structural features. In this enhanced setup, we implement two distinct lower blocks: M_{L_1} for node features and M_{L_2} for structural features. The input for this double hierarchical design is given by:

$$U_G = \text{concat}(U^{AE}v_1, U^X v_1, \cdots, U^{AE}v_n, U^X v_n, Q_G)$$

Table 18: **Comparison of Model Performance by Design Configuration.** Accuracy is used as the metric. This table presents performance metrics across different datasets, distinguishing between Hierarchical and Double Hierarchical design models.

		Double Hierarchical Design		Hierarchical Design
Dataset	Type	1 Lower Block	2 Lower Blocks	1 Lower Block
Pubmed	Node	**94.25**	93.9	92.9
Cora	Node	87.8	**88.3**	86.1
WN18RR	Link	**97.6**	97.5	97.3

This arrangement allows each lower block to specialize, thereby enhancing their processing capabilities on their respective feature types.

From Table 18, we note a slight performance advantage with the double hierarchical design. This design enables the model to more effectively differentiate between node features and structural elements, as these are processed independently in the input, leading to improved performance. The double hierarchical design exhibits comparable results whether using one or two lower blocks. Given the similar performance outcomes, we opt for a single lower block due to its lower parameter count—using two blocks would nearly double the parameters from 86M to 150M. Therefore, in scenarios where parameter efficiency is critical, the double hierarchical design with a single lower block is preferable.

G Limitations, Challenges, and Perspectives

G.1 Limitations

The most significant limitation of our current methodology lies in its lack of zero- and few-shot learning capabilities. Recent advancements in Large Language Models (LLMs) have shown exceptional proficiency in zero- and few-shot scenarios, suggesting an urgent need for research aimed at integrating these capabilities into our approach. An initial attempt to address this, described in Appendix D.2, involves using our model as an encoder coupled with a powerful LLM decoder through prefix tuning. While this approach enhances fine-tuning efficacy, it falls short in generalizing few-shot abilities.

Powerful decoder based LLMs can be used in the future leveraging a similar local to global architecture (using similar attention masks). Earlier layers can be set to focus on tokens of the same node (mimicking intra-node attention). Due to the Causal attention used in decoder LLMs, the last token in every node's description can be either directly be used as the node token in upper block or after pooling with other tokens of same node, mimicking inter-node attention. However, more research is needed and we leave this to future work.

G.2 Challenges

A notable challenge in enhancing our model involves rethinking the attention mechanisms employed in LLMs. Our model benefits from a unique local and global attention scheme, which could inform modifications to the attention masks in LLMs. For example, adapting Transformer block architectures within LLMs to split the layers into two distinct blocks—one focusing exclusively on prior tokens of the current node (lower block) and the other emphasizing a single embedding for every node (upper block)—could be a strategy. However, this structural modification is complex to code and train on LLMs, and it demands substantial computational resources and algorithmic innovation.

G.3 Perspectives

Hybrid models that combine the structure analysis of Graph Neural Networks (GNNs) with the language skills of Large Language Models (LLMs) show great promise for creating stronger systems. These models use the broad abilities of LLMs to work well across different areas, helping to overcome the specific limitations of

traditional GNN architectures. Such models are suited for a wide range of graph-related tasks in real-world settings, compensating for the limitations of GNNs, which usually have only a few million parameters and don't always perform consistently across different fields. This issue highlights the need for better encoding mechanisms that can represent graph data effectively, whether it's for knowledge graphs, molecular structures, or social networks.

Despite increasing interest and some early successes, there are still major challenges, especially in making these models work well across very different areas. Most current research focuses on node classification tasks, which don't fully show what these hybrid models can do in broader applications. Additionally, tests of these models on various graph reasoning tasks are rare, and the results haven't yet shown major breakthroughs. This points to a clear need for more focused research to truly understand these models' abilities to interpret complex structures, identifying it as a key area for future developments.

In conclusion, while our model introduces innovative solutions to graph data analysis, the path forward involves addressing its scalability to zero-shot learning, enhancing its integration with LLM architectures, and expanding its adaptability to diverse and complex graph structures. These developments will not only advance the theoretical foundations of graph neural networks but also expand their applicability and effectiveness in practical scenarios.

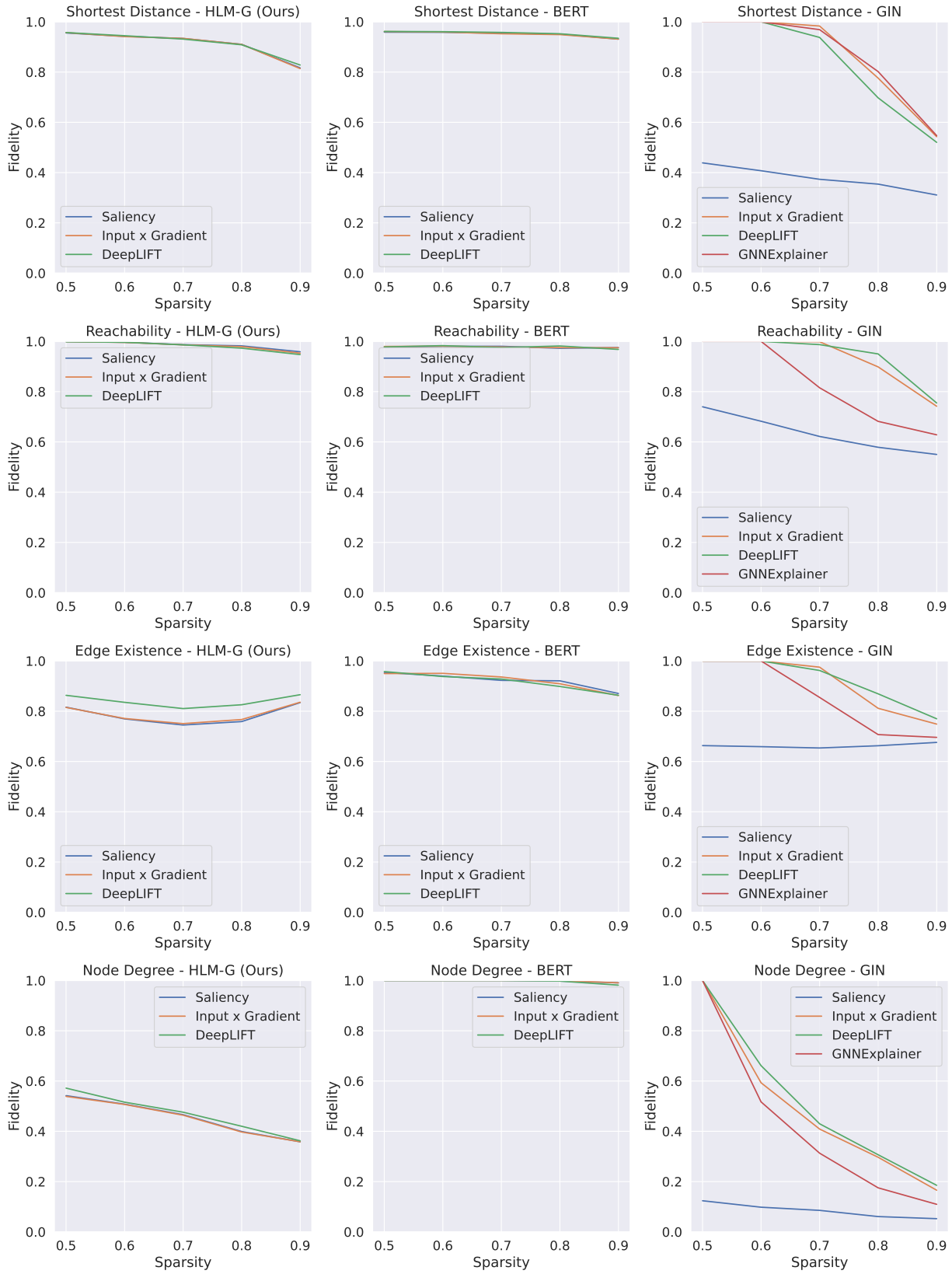

Figure 4: **Fidelity results.** This figure measures the faithfulness of 4 explainers to 3 models using Fidelity scores across different Sparsities. Results should be compared across different explainers within the same dataset and method.

Legend: Negative Neutral Positive

True Label	Predicted Label	Attribution Label	Attribution Score	Word Importance
4	4 (0.77)	4	7.33	node 0 is connected to nodes 15 , 27 , 32 and 37 . node 1 is connected to nodes 2 , 5 , 6 , 8 , 13 , 24 and 36 . node 2 is connected to nodes 1 , 5 , 22 , 24 and 38 . node 3 is connected to nodes 8 , 13 , 19 , 23 and 29 . node 4 is connected to node 27 . node 5 is connected to nodes 1 , 2 , 8 , 12 , 16 , 17 , 27 , 30 , 31 and 37 . node 6 is connected to nodes 1 and 18 . node 7 is connected to nodes 10 , 14 , 22 and 26 . node 8 is connected to nodes 1 , 3 , 5 , 11 , 14 , 23 and 30 . node 9 is connected to nodes 21 and 34 . node 10 is connected to nodes 7 , 12 , 15 , 17 , 33 and 35 . node 11 is connected to nodes 8 , 24 and 26 . node 12 is connected to nodes 5 , 10 , 22 and 30 . node 13 is connected to nodes 1 , 3 , 22 and 23 . node 14 is connected to nodes 7 , 8 , 18 , 19 and 27 . node 15 is connected to nodes 0 , 10 , 22 , 26 , 34 and 37 . node 16 is connected to nodes 5 , 19 , 32 and 36 . node 17 is connected to nodes 5 , 10 , 22 , 27 and 34 . node 18 is connected to nodes 6 , 14 and 32 . node 19 is connected to nodes 3 , 14 , 16 , 22 , 24 and 30 . node 20 is connected to nodes 22 , 27 , 28 , 31 and 32 . node 21 is connected to nodes 9 and 25 . node 22 is connected to nodes 2 , 7 , 12 , 13 , 15 , 17 , 19 , 20 , 23 , 24 , 32 and 34 . node 23 is connected to nodes 3 , 8 , 13 , 22 and 34 . node 24 is connected to nodes 1 , 2 , 11 , 19 and 22 . node 25 is connected to node 21 . node 26 is connected to nodes 7 , 11 , 15 and 37 . node 27 is connected to nodes 0 , 4 , 5 , 14 , 17 and 20 . node 28 is connected to node 20 . node 29 is connected to node 3 . node 30 is connected to nodes 5 , 8 , 12 and 19 . node 31 is connected to nodes 5 and 20 . node 32 is connected to nodes 0 , 16 , 18 , 20 and 22 . node 33 is connected to nodes 10 and 38 . node 34 is connected to nodes 9 , 15 , 17 , 22 , 23 and 38 . node 35 is connected to node 10 . node 36 is connected to nodes 1 and 16 . node 37 is connected to nodes 0 , 5 , 15 , 26 and 38 . node 38 is connected to nodes 2 , 33 , 34 and 37 . what is the degree of node 0 ?

Figure 5: **Interpretation visualization of HLM-G (ours) on the node degree dataset.**

Legend: Negative Neutral Positive

True Label	Predicted Label	Attribution Label	Attribution Score	Word Importance
4	4 (1.00)	4	3.21	node 0 is connected to nodes 15 , 27 , 32 and 37 . node 1 is connected to nodes 2 , 5 , 6 , 8 , 13 , 24 and 36 . node 2 is connected to nodes 1 , 5 , 22 , 24 and 38 . node 3 is connected to nodes 8 , 13 , 19 , 23 and 29 . node 4 is connected to node 27 . node 5 is connected to nodes 1 , 2 , 8 , 12 , 16 , 17 , 27 , 30 , 31 and 37 . node 6 is connected to nodes 1 and 18 . node 7 is connected to nodes 10 , 14 , 22 and 26 . node 8 is connected to nodes 1 , 3 , 5 , 11 , 14 , 23 and 30 . node 9 is connected to nodes 21 and 34 . node 10 is connected to nodes 7 , 12 , 15 , 17 , 33 and 35 . node 11 is connected to nodes 8 , 24 and 26 . node 12 is connected to nodes 5 , 10 , 22 and 30 . node 13 is connected to nodes 1 , 3 , 22 and 23 . node 14 is connected to nodes 7 , 8 , 18 , 19 and 27 . node 15 is connected to nodes 0 , 10 , 22 , 26 , 34 and 37 . node 16 is connected to nodes 5 , 19 , 32 and 36 . node 17 is connected to nodes 5 , 10 , 22 , 27 and 34 . node 18 is connected to nodes 6 , 14 and 32 . node 19 is connected to nodes 3 , 14 , 16 , 22 , 24 and 30 . node 20 is connected to nodes 22 , 27 , 28 , 31 and 32 . node 21 is connected to nodes 9 and 25 . node 22 is connected to nodes 2 , 7 , 12 , 13 , 15 , 17 , 19 , 20 , 23 , 24 , 32 and 34 . node 23 is connected to nodes 3 , 8 , 13 , 22 and 34 . node 24 is connected to nodes 1 , 2 , 11 , 19 and 22 . node 25 is connected to node 21 . node 26 is connected to nodes 7 , 11 , 15 and 37 . node 27 is connected to nodes 0 , 4 , 5 , 14 , 17 and 20 . node 28 is connected to node 20 . node 29 is connected to node 3 . node 30 is connected to nodes 5 , 8 , 12 and 19 . node 31 is connected to nodes 5 and 20 . node 32 is connected to nodes 0 , 16 , 18 , 20 and 22 . node 33 is connected to nodes 10 and 38 . node 34 is connected to nodes 9 , 15 , 17 , 22 , 23 and 38 . node 35 is connected to node 10 . node 36 is connected to nodes 1 and 16 . node 37 is connected to nodes 0 , 5 , 15 , 26 and 38 . node 38 is connected to nodes 2 , 33 , 34 and 37 . what is the degree of node 0 ?

Figure 6: **Interpretation visualization of BERT on the node degree dataset.**